Infrared regime of SU(2) with one adjoint Dirac flavor

Andreas Athenodorou, Ed Bennett, Georg Bergner, and Biagio Lucini

Phys. Rev. D **91**, 114508 — Published 18 June 2015

DOI: 10.1103/PhysRevD.91.114508

The infrared regime of SU(2) with one adjoint Dirac flavour

Andreas Athenodorou,[1, 2, *] Ed Bennett,[1, †] Georg Bergner,[3, ‡] and Biagio Lucini[1, §]

[1] *Department of Physics, Swansea University, Singleton Park, Swansea SA2 8PP, UK*
[2] *Department of Physics, University of Cyprus, POB 20537, 1678 Nicosia, Cyprus*
[3] *Universität Bern, Institut für Theoretische Physik, Sidlerstr. 5, CH-3012 Bern, Switzerland*

SU(2) gauge theory with one Dirac flavour in the adjoint representation is investigated on a lattice. Initial results for the gluonic and mesonic spectrum, static potential from Wilson and Polyakov loops, and the anomalous dimension of the fermionic condensate from the Dirac mode number are presented. The results found are not consistent with conventional confining behaviour, instead tentatively pointing towards a theory lying within or very near the onset of the conformal window, with the anomalous dimension of the fermionic condensate in the range $0.9 \lesssim \gamma_* \lesssim 0.95$. The implications of our work for building a viable theory of strongly interacting dynamics beyond the standard model are discussed.

PACS numbers: 11.15.Ha and 12.60.Nz

I. INTRODUCTION

Even after the recent experimental identification of the Higgs particle [1, 2], the existence of a new fundamental interaction of which the Higgs sector is the low energy manifestation is still an open problem. Among the proposed possibilities, novel strong dynamics [3–7] is still a good candidate for a possible fundamental mechanism of electroweak symmetry breaking. It is generally believed that this new strong interaction is able to explain the observed electroweak symmetry breaking phenomenology if the following three conditions are met: (1) the theory must be near the onset of the conformal window; (2) the anomalous dimension of the chiral condensate must be of order one; and (3) a parametrically light scalar (the would-be Higgs boson) must be in the spectrum. The first two conditions [8, 9] are needed for compatibility with electroweak precision data [10], while the third condition is determined by the direct observation of the Higgs boson and no other previously unknown nearby state. Until very recently, even the possible existence of a strongly interacting quantum field theory for which any of those conditions arose was unclear. In the last few years, much progress has been achieved on these theoretical questions, thanks to a combination of methods and techniques. A crucial role has been played by numerical investigations using lattice techniques, which—among other results—have pinned down an example of a gauge theory in the conformal window, namely SU(2) gauge theory with two adjoint Dirac flavours [11–19] (see [20–23] for earlier simulations of the model). Although conformal strong dynamics can still explain electroweak symmetry breaking, an anomalous dimension around one is required [24]. This condition rules out a possible phenomenological role played by SU(2) with two adjoint Dirac flavours in its simplest version: in fact, the most recent measurements of the anomalous dimension $\gamma^\star$ for this model give $\gamma^\star = 0.38(2)$ [25], which is well below the acceptable value. With the possible exception of SU(3) with eight flavours [26], whose infrared behaviour needs to be better explored, all other candidate near-conformal theories studied so far have an anomalous dimension that is too small (see [27, 28] for recent overviews of lattice calculations).

At this stage, it is a fundamental problem to understand whether large anomalous dimensions can arise in the context of conformal or near-conformal gauge theories. Although the anomalous dimension is small at the perturbative zeros of the beta function, large anomalous dimensions might arise near or at the lower end of the conformal window. Whether these conjectured large anomalous dimensions arise is a crucial question not only for building realistic models of electroweak symmetry breaking based on a novel strong interaction, but also in the more general context of the physics of non-Abelian gauge theories. As mentioned above, for SU(2) gauge theories with adjoint Dirac fermions, lattice studies show that the model with two flavours is infrared conformal with a small anomalous dimension. Hence, a remaining potential way to observe a large anomalous dimension is to consider the case of a single Dirac flavour, or equivalently two Majorana (or Weyl) fermions.

Analytically, this theory could be seen as the large scalar mass limit of $\mathcal{N} = 2$ super Yang–Mills with gauge group SU(2), with supersymmetry completely broken by a non-zero mass term for the scalar. Despite the existence of an interpolating parameter (in this specific case, the mass of the scalar) confinement in $\mathcal{N} = 2$ super Yang–Mills theory does not trivially imply confinement in the limit in which the scalar decouples. In $\mathcal{N} = 2$ super Yang–Mills, confinement is known to arise through the dual superconductor mechanism resulting from magnetic monopole condensation [29]. However, this mechanism does not immediately generalise to the non-supersymmetric case, since non-trivial effects (e.g.

*Electronic address: athenodorou.andreas@ucy.ac.cy
†Electronic address: e.j.bennett@swan.ac.uk
‡Electronic address: g.bergner@uni-muenster.de
§Electronic address: B.Lucini@swan.ac.uk

the fate of the monopoles when decoupling the scalar) enter the interpolating theory. Exploratory lattice studies exist for SU(N) gauge theory with a single adjoint Dirac flavour in the large-N limit [30–32]. These works, which exploit large-N volume reduction, do not give yet a clear picture of the infrared behaviour of the theory. In addition, although perturbatively the N-dependence of the β-function of theories with adjoint fermions is mild [33], in principle the results of those studies might not translate immediately to the model with two colors.

In this work, we present a first-principles investigation of the model using numerical Monte Carlo studies of the theory discretised on a spacetime lattice. The central result of our work is that the infrared regime of the system is compatible with a conformal or near-conformal behaviour, but not with a conventional QCD-like scenario in which chiral symmetry breaking takes place. Furthermore, the anomalous dimension (measured with two independent methods) turns out to be 0.925(25).

The rest of the paper is organised as follow. In Sect. II we present the model and the setup of our numerical investigations. Numerical results will then be presented in Sect. III. Sect. IV discusses the implications of our investigation and possible directions of future studies. Finally, a summary will be presented in Sec. V. Some preliminary results were already presented in [34].

II. THE MODEL

We consider an SU(2) gauge theory with a single Dirac flavour in the adjoint representation with mass m. Eventually, we would be interested in understanding the properties of the theory in the massless limit; however, numerical simulations require a non-zero fermion mass. Hence, we deform the theory with a small fermion mass, and study how the system approaches the massless limit. We stress from the outset that regardless of the phase of the theory at zero fermion mass, with a finite mass term chiral symmetry is always broken, since the mass is a relevant direction for the renormalization group trajectory. The expectations are that if chiral symmetry is broken in the massless limit, the response of the model to a small varying mass will be described by chiral perturbation theory, while if the theory is conformal the data will be in accord with the predictions derived from a mass-deformed conformal gauge theory. A third possibility is that the system is in the confined phase, but close to the onset of the conformal window. In this case, it will show mass-deformed conformal behaviour in an intermediate energy regime between a chiral symmetry breaking scale $\Lambda_{\rm IR}$ and the ultraviolet perturbative scale $\Lambda_{\rm UV}$, while chiral perturbation theory will correctly describe the theory for energies below $\Lambda_{\rm IR}$. The latter possibility, referred commonly as *near-conformality* or *walking behaviour*, would be phenomenologically interesting, since theories near the onset of the conformal window are relevant for gaining an understanding of strongly interacting dynamics beyond the standard model as the mechanism of electroweak symmetry breaking.

In the following subsections, we describe the field content of the theory, the chiral symmetry breaking pattern, and the resulting spectrum.

A. Field content

In Minkowskian space, the Lagrangian of the system is given by

$$\mathcal{L} = \overline{\psi}(x)\left(i\not{D} - m\right)\psi(x) - \frac{1}{2}\mathrm{Tr}\left(G_{\mu\nu}(x)G^{\mu\nu}(x)\right) \ , \quad (1)$$

where $\not{D} = \left(\partial_\mu + igA_\mu(x)\right)\gamma^\mu$, γ_μ are the Dirac matrices, $A_\mu(x) = \sum_a T^a A^a_\mu(x)$ with $a = 1,2,3$, and the T_a are the generators of SU(2) in the adjoint representation (i.e. the generators of SO(3)). $G_{\mu\nu} = \partial_\mu A_\nu(x) - \partial_\nu A_\mu(x) + ig[A_\mu(x), A_\nu(x)]$, with g the gauge coupling of the theory, is the field tensor, and the trace is taken over the gauge group. Our notations for the Dirac algebra matrices and derived symmetry operators are reported in Appendix A.

Since the theory contains a single (Dirac) flavour, described by the spinor $\psi(x)$, at first sight the flavour structure of Eq. (1) would seem trivial. However, since the adjoint representation is real, it does not mix the real and the imaginary part of the Dirac spinor. More explicitly, if C is the Dirac matrix implementing charge conjugation, we can decompose the Dirac spinor in Majorana components

$$\xi_+ = \frac{\psi + C\overline{\psi}^{\rm T}}{\sqrt{2}} \ , \qquad \xi_- = \frac{\psi - C\overline{\psi}^{\rm T}}{\sqrt{2}i} \ , \quad (2)$$

such that

$$\psi = \frac{1}{\sqrt{2}}(\xi_+ + i\xi_-) \ , \quad (3)$$

with both ξ_+ and ξ_- being invariant under charge conjugation symmetry by construction. Eq. (1) can now be rewritten as

$$\mathcal{L} = \frac{1}{2}\sum_k \bar{\xi}_k(x)\left(i\not{D} - m\right)\xi_k(x) - \frac{1}{2}\mathrm{Tr}\left(G_{\mu\nu}(x)G^{\mu\nu}(x)\right) , \quad (4)$$

where $k = +, -$. This flavour structure (in terms of the Majorana components) gives rise to a non-trivial chiral symmetry breaking pattern.

B. Chiral symmetry breaking pattern

In the notation usually applied in considerations of supersymmetry, the fermion part of the Lagrangian is written as

$$\begin{aligned} &\sum_k \left[(\bar{\zeta}_k)_{\dot\alpha}(\bar\sigma^\mu)^{\dot\alpha\beta}D_\mu(\zeta_k)_\beta + \frac{m}{2}((\zeta_k)^\alpha(\zeta_k)_\alpha + h.c.)\right] \\ = &\sum_k \left[\zeta_k^\dagger\bar\sigma^\mu D_\mu\zeta_k + \frac{m}{2}(\zeta_k^{\rm T}\epsilon^{\rm T}\zeta_k + h.c.)\right] \ , \end{aligned} \quad (5)$$

with $\alpha, \beta = 1, 2$ spin indices[1], Majorana spinors ζ_k in the Weyl representation

$$\xi_k = \begin{pmatrix} \zeta \\ \epsilon\zeta^* \end{pmatrix}_k = \begin{pmatrix} \zeta_\alpha \\ \bar{\zeta}^{\dot{\alpha}} \end{pmatrix}_k , \tag{6}$$

and $\epsilon = i\sigma_2$. The lower component of the Majorana spinor can be derived from the upper one using the above expression. Therefore we can ignore the lower components and form a $4N_\mathrm{f}$ component vector out of the two upper Weyl components of each Majorana flavour, for $N_\mathrm{f} = 1$ we get

$$\eta = \begin{pmatrix} \zeta_1 \\ \zeta_2 \end{pmatrix} . \tag{7}$$

In the zero mass limit the action has a $\mathrm{U}(1)_A \otimes \mathrm{SU}(2N_\mathrm{f})$ symmetry. The $\mathrm{SU}(2N_\mathrm{f})$ part rotates the upper and lower two components of η into each other. The $\mathrm{U}(1)_A$ part is broken by the anomaly down to a discrete Z_{2N_c}. The remaining $Z_{2N_\mathrm{c}} \otimes \mathrm{SU}(2N_\mathrm{f})$ is subject to a spontaneous symmetry breaking if there is a non-zero expectation value of the fermion condensate. The condensate and the fermion mass term are invariant under the subgroup $Z_2 \otimes \mathrm{SO}(2N_\mathrm{f})$. This is the remaining exact symmetry group if there is a spontaneous symmetry breaking. Therefore, the chiral symmetry breaking pattern is

$$\mathrm{SU}(2N_\mathrm{f}) \mapsto \mathrm{SO}(2N_\mathrm{f}) . \tag{8}$$

Hence, if chiral symmetry is spontaneously broken, there are two Goldstone bosons in this model, corresponding to the two generators of the broken part of the symmetry. In the present case of $N_\mathrm{f} = 1$ the complete flavour symmetry SU(2) has generators $\sigma_i/2$. In order to mark the difference with the σ_i acting on the two indices of the Weyl spinor, we call the generators in flavour space $\tau_i = \sigma_i$. The unbroken SO(2) is generated by $\tau_2/2 = \sigma_2/2$ and is equivalent to U(1).

We want to arrive at a diagonal representation of the unbroken symmetry. Therefore we apply the following unitary transformation on η

$$\chi = \frac{1}{\sqrt{2}} \begin{pmatrix} 1 & i \\ i & 1 \end{pmatrix} \eta = \frac{1}{\sqrt{2}} (1 + i\tau_1)\eta = \begin{pmatrix} \chi_1 \\ \chi_2 \end{pmatrix} \tag{9}$$

$$= P_\mathrm{L}\psi + P_\mathrm{R}(-iC)\psi^* = \begin{pmatrix} \psi_\mathrm{L} \\ -\sigma_2\psi_\mathrm{R}^* \end{pmatrix} . \tag{10}$$

The P_R and P_L are the projectors on the left handed (ψ_L) and right handed (ψ_R) part of the Dirac spinor. The advantage of this transformation is that the unbroken generator is now the diagonal $\tau_3/2$ and the unbroken SO(2) subgroup can be rewritten as

$$U = \cos\alpha + i\tau_3 \sin\alpha = e^{i\alpha\tau_3} . \tag{11}$$

In the Majorana formulation, there is no U(1) symmetry for each of the two Majorana flavours and hence one would naturally relate the unbroken symmetry to the isospin in QCD. In the Dirac notation the unbroken symmetry is, however, the $\mathrm{U}(1)_V$ of charge conservation. Therefore in the following we refer to it as baryon symmetry. Hence, in addition to parity, the baryon charge related to the unbroken part of the chiral symmetry can be used to classify the spectrum of the theory in the broken phase. At this point, it is worth stressing again that chiral symmetry breaking is expected to arise as a soft breaking at finite fermion mass, independently of the phase of the massless theory.

While the residual symmetry is diagonal, in this basis parity is expressed in terms of a combination of charge conjugation (σ_2) and flavour rotation (τ_2). In fact, the action of parity in the original basis

$$\psi(t, \vec{x}) \mapsto \gamma_0\psi(t, -\vec{x}) , \tag{12}$$

$$\overline{\psi}(t, \vec{x}) \mapsto \overline{\psi}(t, -\vec{x})\gamma_0 , \tag{13}$$

determines the transformations

$$\chi(t, \vec{x}) \mapsto i\sigma_2\tau_2\chi^*(t, -\vec{x}) , \tag{14}$$

$$\chi^\dagger(t, \vec{x}) \mapsto -\chi^\mathrm{T}(t, -\vec{x})i\sigma_2\tau_2 . \tag{15}$$

In order to clarify the notation, we derive explicitly the chiral symmetry breaking pattern directly in this basis. The chiral symmetry group SU(2) commutes with the parity transformation, since for $U \in \mathrm{SU}(2)$

$$U(i\tau_2) = (i\tau_2)U^* . \tag{16}$$

The chiral condensate represented in the different bases of flavour and Dirac space has the following form

$$\overline{\psi}\psi = \frac{1}{2}\sum_k (\zeta_k^\mathrm{T}\epsilon^\mathrm{T}\zeta_k + h.c.) \tag{17}$$

$$= \frac{1}{2}(\eta^\mathrm{T}\epsilon^\mathrm{T}\eta + h.c.) \tag{18}$$

$$= \psi_\mathrm{L}^\dagger\psi_\mathrm{R} + \psi_\mathrm{R}^\dagger\psi_\mathrm{L} \tag{19}$$

$$= \chi_1^\dagger\sigma_2\chi_2^* + \chi_2^\mathrm{T}\sigma\chi_1 \tag{20}$$

$$= \frac{1}{2}\left(\chi^\mathrm{T}\tau_1\sigma_2\chi + \chi^\dagger\tau_1\sigma_2\chi^*\right) . \tag{21}$$

From the last line, one can see that when the degrees of freedom are chosen to be χ and $\chi^\dagger$, the chiral condensate is left invariant under the subgroup of U matrices that satisfy

$$U^\mathrm{T}\tau_1 U = \tau_1 , \tag{22}$$

which is the SO(2) subgroup generated by τ_3, Eq. (11).

Note that the symmetry breaking pattern shown here is used in [35] to derive a partially quenched chiral perturbation theory for supersymmetric Yang–Mills theory[2].

[1] We have made use of the dotted-undotted notation commonly found in supersymmetry, for which we refer to the specialised literature.

[2] We remark that [35] uses a different convention on parity. See Appendix B for a brief discussion of the two conventions.

The analysis relies on the small mass of the Goldstone bosons compared to the other states in the theory. This needs to be confronted with our results: in a conformal or near-conformal scenario the theory develops no relevant intrinsic mass scale and the expected hierarchy of masses is lost.

C. The spectrum

In order to understand the phase of the theory from the point of view of the chiral symmetry, we focus our attention on bilinear fermionic operators, which can be seen as creation and annihilation operators of physical states that play a crucial role in establishing the chiral properties of the system.

The bilinear fermionic operators considered in this study are shown in Tab. I. For convenience, they are represented in the Dirac notation ("Dirac bilinears") and in the Majorana notation ("Majorana bilinears"). For the latter case, we introduce the naming convention

$$O_{lk}(\Gamma) = \bar{\xi}_l \Gamma \xi_k \ , \tag{23}$$

where the ξ are the two Majorana flavours (labeled by $k, l = +, -$) and Γ is a Dirac matrix or a product of Dirac matrices. Both the Majorana and the Dirac form has some advantage: the Dirac representation allows us to identify easily the spin quantum numbers (reported in column "Spin") and the parity, while the Majorana notation exposes the flavour structure and bridges with the terminology often used in supersymmetry. Straightforward algebra enables one to obtain the expression in one notation given the expression in the other. For the sake of simplicity, we have omitted the Weyl notation, which is particularly suited for the $SU(2)$ quantum numbers. The Weyl notation can be easily obtained from the Dirac notation. For instance, one finds that

$$\frac{1}{2}(\psi^{\mathrm{T}} C\gamma_5\gamma_0\psi + \psi^\dagger C\gamma_5\gamma_0\psi^*) = \chi^\dagger \tau_2 \chi \ , \tag{24}$$

i.e. the Weyl bilinear $\chi^\dagger\tau_2\chi$, transforming under the 3^+ representation of $\mathrm{SU}(2)^P$, is half the sum of the Dirac bilinears $\psi^{\mathrm{T}} C\gamma_5\gamma_0\psi$ and $\psi^\dagger C\gamma_5\gamma_0\psi^*$, both in the irreduciple representation 3^+ of the original flavour group, but carrying baryon charge $+2$ and -2 respectively.

As usual, masses are extracted by looking at the large-distance exponential decay of correlators between operators with the same quantum numbers. For fermionic bound states, we are interested in the $\mathrm{U}(1)^P$ quantum numbers. When expressing the relevant correlators in the original Dirac notation, we use the conventional language of Lattice QCD. In particular, the words singlet and triplet do not refer to a QCD-like isospin symmetry, which is not defined in this theory. Here they stand for whether fermion disconnected diagrams need to be evaluated (singlet case) or not (as it happens for the triplet). These contributions might appear in different

Spin	$\mathrm{SU}(2)^P$	Dirac bilinears	Majorana bilinears	$\mathrm{U}(1)^P$	Name	Correlators
(pseudo)scalars	1^-	$\bar\psi\gamma_0\gamma_5\psi$	$O_{++}(\gamma_0\gamma_5) + O_{--}(\gamma_0\gamma_5)$	0^-	pseudoscalar meson	singlet γ_5, $\gamma_0\gamma_5$
	3^-	$\bar\psi\gamma_5\psi$	$O_{++}(\gamma_5) + O_{--}(\gamma_5)$			
		$\psi^{\mathrm{T}} C\psi$	$O_{++}(1) - O_{--}(1) + 2iO_{+-}(1)$	2^-	pseudoscalar (anti)baryon	triplet 1
		$\psi^\dagger C\psi^*$	$O_{++}(1) - O_{--}(1) - 2iO_{+-}(1)$	-2^-		
	3^+	$\bar\psi\psi$; $\bar\psi\gamma_0\psi$	$O_{++}(1) + O_{--}(1)$; $O_{+-}(\gamma_0)$	0^+	scalar meson	singlet 1, γ_0
		$\psi^{\mathrm{T}} C\gamma_5\psi$; $\psi^{\mathrm{T}} C\gamma_5\gamma_0\psi$	$O_{++}(\gamma_5) - O_{--}(\gamma_5) + 2iO_{+-}(\gamma_5)$; $O_{++}(\gamma_5\gamma_0) - O_{--}(\gamma_5\gamma_0) + 2iO_{+-}(\gamma_5\gamma_0)$	2^+	scalar (anti)baryon	triplet γ_5, $\gamma_0\gamma_5$
		$\psi^\dagger C\gamma_5\psi^*$; $\psi^\dagger C\gamma_5\gamma_0\psi^*$	$O_{++}(\gamma_5) - O_{--}(\gamma_5) - 2iO_{+-}(\gamma_5)$; $O_{++}(\gamma_5\gamma_0) - O_{--}(\gamma_5\gamma_0) - 2iO_{+-}(\gamma_5\gamma_0)$	-2^+		
(axial) vectors	1^+	$\bar\psi\gamma_5\vec\gamma\psi$; $\bar\psi\gamma_0\gamma_5\vec\gamma\psi$	$O_{++}(\gamma_5\vec\gamma) + O_{--}(\gamma_5\vec\gamma)$; $O_{+-}(\gamma_0\gamma_5\vec\gamma)$	0^+	axial vector meson	singlet $\gamma_5\vec\gamma$, $\gamma_0\gamma_5\vec\gamma$
	1^-	$\bar\psi\gamma_0\vec\gamma\psi$	$O_{+-}(\gamma_0\vec\gamma)$	0^-	vector meson	singlet $\vec\gamma$, $\gamma_0\vec\gamma$
	3^-	$\bar\psi\vec\gamma\psi$	$O_{+-}(\vec\gamma)$			
		$\psi^{\mathrm{T}} C\gamma_5\vec\gamma\psi$	$O_{++}(\gamma_5\vec\gamma) - O_{--}(\gamma_5\vec\gamma) + 2iO_{+-}(\gamma_5\vec\gamma)$	2^-	vector (anti)baryon	triplet $\gamma_5\vec\gamma$
		$\psi^\dagger C\gamma_5\vec\gamma\psi^*$	$O_{++}(\gamma_5\vec\gamma) - O_{--}(\gamma_5\vec\gamma) - 2iO_{+-}(\gamma_5\vec\gamma)$	-2^-		

TABLE I: Dirac and Majorana bilinears classified according to their $\mathrm{SU}(2)^P$ and $\mathrm{U}(1)^P$ quantum numbers, together with the correlators used for the calculations of the corresponding masses.

cases than what one expects from QCD. For instance, to obtain a pseudoscalar meson in our theory it is, as in one flavour QCD, unavoidable to compute disconnected contributions. The terminology is further discussed in Appendix C. The correlators with the naming convention inherited from QCD that are needed to compute masses in a given channel in terms of the single Dirac flavour are indicated in the last column of Tab. I. The naming of the states (column "Name"), which will be used as a handy reference in the following, is instead derived from the U(1) quantum numbers, which characterise the physical states. In particular, 2 indicates the baryon with charge $q = 2$, -2 the antibaryon with charge $q = -2$ and zero the scalar/vector meson (or pseudoscalar/pseudovector meson, if the parity is negative)[3].

As mentioned above, the SU(2) quantum numbers can be easily read in the Weyl basis. We have indicated with 1 the singlet and with 3 the triplet of the SU(2) flavour group. If chiral symmetry is broken, the Goldstone bosons are the charged baryons that belong to the positive-parity triplet of the original flavour group (quantum numbers 3^+). Their $\mathrm{U}(1)^P$ quantum numbers are $\pm 2^+$. In the Dirac notation, operators carrying the wanted quantum numbers are $\psi^{\mathrm{T}} C\gamma_5\gamma_0\psi$ and $\psi^\dagger C\gamma_5\gamma_0\psi^*$. Hence, correlators of those operators are going to play a central role: if they identify parametrically light particles as the Lagrangian fermion mass is sent to zero, there will be a clear support for QCD-like chiral symmetry breaking, otherwise we will get an indication that the theory may be in a less familiar phase or regime.

It is worth remarking that when it comes to the definition of physical states, each choice of the fermion notation has advantages and disadvantages. In particular, in the Majorana notation, states with a well-defined baryon charge can be obtained only by combining correlators of different bilinears. Calculations of correlators can be carried out using elementary properties of the Dirac algebra and will not be discussed any further. For some explicit examples, we refer to [34].

In addition to purely fermionic operators, one can consider gluonic operators and mixed gluonic-fermionic operators. Calculations involving those operators do not present any relevant difference with respect to similar calculations performed earlier and reported in the literature, to which we refer for further technical details (see e.g. [11, 16, 36]). Since the physical states contributing to a correlator in a particular channel are selected solely by their quantum numbers, in general the large distance exponential decay of correlators with the same quantum numbers is dominated by the same mass, which is the mass corresponding to the ground state in that channel[4]. This is particularly relevant for the scalar, which should emerge both in a calculation involving purely fermionic operators and in a calculation involving purely gluonic operators with quantum numbers[5] $J^P = 0^+$. This channel is particularly important for phenomenology, as in models of strongly interacting dynamics beyond the standard model it is identified with the Higgs boson of the standard model itself. For a novel strongly interacting theory to be compatible with the latest experimental findings, the scalar must turn out to be lighter than the other particles. One of the central results of our calculation is a sufficiently precise measurement of the notoriously noisy scalar channel that enables us to assess with enough accuracy what is the mass difference between the scalar and the nearest particle in the spectrum, as we shall see in the following section.

III. RESULTS

The action of the discretised model used in our numerical study is given by

$$S = S_{\mathrm{G}} + S_{\mathrm{F}} \tag{25}$$

where

$$S_{\mathrm{G}} = \beta \sum_p \mathrm{Tr}\left[1 - U(p)\right] \tag{26}$$

and

$$S_{\mathrm{F}} = \sum_{x,y} \overline{\psi}(x) D(x,y) \psi(y), \tag{27}$$

are respectively the pure gauge part (Wilson action) and the fermionic contribution. Here $U(p)$ is the lattice plaquette and

$$\begin{aligned} D(x,y) = \delta_{x,y} - \kappa \left[\left(1-\gamma_\mu\right) U_\mu(x) \delta_{y,x+\mu} \right. \\ \left. + \left(1+\gamma_\mu\right) U_\mu^\dagger(x-\mu) \delta_{y,x-\mu} \right] \end{aligned} \tag{28}$$

is the massive Dirac operator in the Wilson lattice discretisation of fermion fields. $\kappa = 1/(8 + 2am)$ is the hopping parameter, a the lattice spacing and m the

[3] The states that are called *baryons* in this work are more often referred to as *diquarks* in the literature of studies of gauge theories based on a (pseudo-)real gauge group (e.g. SU(2), G(2)). The same nomenclature is sometimes used for a real representation of a gauge group (e.g. the adjoint representation). This naming convention is discussed also in Appendix B. We note that also the spin 1/2 state introduced below has a non-trivial baryon charge, and hence is classified as a baryon. However, with the term *(anti-)baryon* we indicate in this work only the states with $q = 2$ ($q = -2$).

[4] However, there are cases in which either kinematics or dynamics prevents some states from appearing in certain correlators. A remarkable example in this category is large-N QCD, for which, for instance, meson correlators do not get contributions from glueballs and viceversa.

[5] We have omitted charge conjugation, which for gauge group SU(2) is always positive.

bare fermion mass. For further details about the lattice model, we refer to [11, 15, 16], where the $N_f = 2$ adjoint fermion case is studied for gauge group SU(2), using similar notations. The algebra relating the various fermion formalisms carries over to the lattice in a straightforward way. The simulations were done using the HiRep code [21]. The Monte Carlo trajectories used for sampling observables were generated using a Rational Hybrid Monte Carlo (RHMC) algorithm [37]. Other details on our simulations are provided in Appendix D.

Correlators among operators can be computed on a spacetime lattice after Euclidean rotation. In particular, if $\vec{x}$ and t are respectively the spatial and temporal components of the position vector x, for a bilinear $\Psi(x)$ we have

$$\lim_{t\to\infty} \sum_{\vec{x}} \langle \overline{\Psi}(\vec{x}_0, t_0)\Psi(\vec{x}, t_0 + t)\rangle \propto e^{-m_\alpha t} \ , \qquad (29)$$

where m_α is the lowest mass with the quantum numbers α carried by Ψ and the sum is over the whole spatial volume.

In our study, we make use of Wilson fermions, for which chiral symmetry is explicitly broken. As a consequence, the fermion mass gets an additive renormalisation term that shifts the chiral point away from zero bare mass. A mass that is only subject to multiplicative renormalisation (and hence is zero at the chiral point) can be defined through the *partially conserved axial current (PCAC)*. Using the Dirac notation, the PCAC mass is defined as the large time limit of

$$am_{\mathrm{PCAC}}(t) = \frac{\sum_{\vec{x}} \left\langle \partial_0 A_0(\vec{x}, t) P(\vec{0}, 0)\right\rangle}{2\sum_{\vec{x}} \left\langle P(\vec{x}, t) P(\vec{0}, 0)\right\rangle} \ , \qquad (30)$$

where

$$A_0(\vec{x}, t) = \overline{\psi}(\vec{x}, t)\gamma_0\gamma_5\psi(\vec{x}, t) \qquad (31)$$

$$P(\vec{x}, t) = \overline{\psi}(\vec{x}, t)\gamma_5\psi(\vec{x}, t) \ , \qquad (32)$$

and the time derivative is discretised using the backward-forward symmetrised lattice difference operator (which is defined as the difference between the values of a function in two neighbour points divided by the lattice spacing). The lattice technology used to define correlators and the m_{PCAC} mass and to compute them on the lattice is by now standard (see e.g. [38] for a more extended treatment).

In our investigation of fermion correlators, we used the $N_f = 1$ Dirac and the Majorana formalism (see e.g. [39, 40] for technical details on lattice computations involving Majorana fermions), in some cases performing the analysis in both ways to cross-validate the result. The analysis code in the Dirac formalism, used for connected contributions to correlators, is based on HiRep, while a code developed for studies of Super Yang–Mills theories [36] has been used for cross-validation of results for triplet contributions, for calculations involving singlets and for spin–gauge composite states. Gluonic observables (and in particular glueball states) have been studied using the techniques exposed in [41]. Our numerical results are reported below.

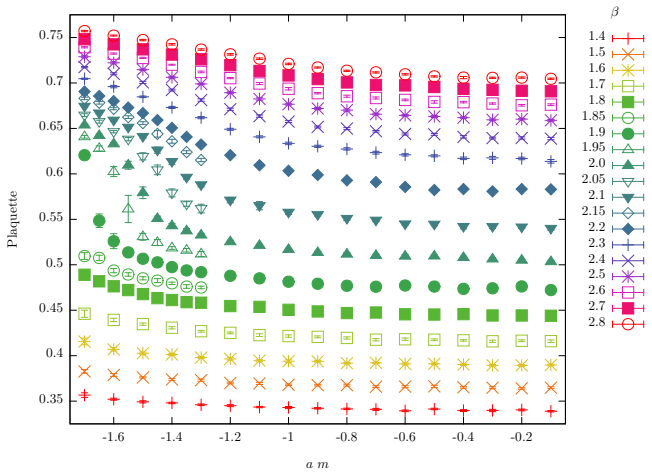

FIG. 1: (Color online) The phase diagram of the theory, showing the average plaquette on a 4^4 lattice at $1.4 \le \beta \le 2.8$, $-1.7 \le am \le -0.1$.

A. Phase diagram

The lattice action describes the physics of the continuum model only in the limit $\beta \to \infty$. The opposite (strong coupling) limit is generally separated from the continuum (below referred to as the "physical region") by a phase transition. The strong coupling phase, dominated by lattice artefacts, is called the *bulk phase*. An order parameter for the transition from the bulk phase to the phase connected to the continuum theory is the plaquette. Simulations aiming at studying continuum physics need to make sure that the parameters are chosen in such a way that the model is in the region connected to the continuum. A simple scan on a small lattice allows us to perform a sensible choice of the parameters.

In the absence of a prior investigation of this theory on the lattice, a study of the lattice phase diagram was necessary to identify the physical region. The average plaquette was considered on a 4^4 lattice, in the ranges $1.4 \le \beta \le 2.8$, $-1.7 \le am \le -0.1$, in steps of 0.1. Once the region of the bulk phase transition was identified, points were added in its neighbourhood to increase the resolution to 0.05. The results, shown in Fig. 1, indicate a bulk phase transition at $\beta \approx 1.9$, $am \approx -1.65$.

In order to simulate near the continuum, a large β would be ideally needed. However, the larger the β the smaller the lattice spacing. Hence, to obtain a lattice of a physically meaningful size a large number of sites in each direction is needed. In practical terms, this will make the simulation computationally very costly, with the cost increasing exponentially with β. Likewise, ide-

TABLE II: The lattices considered in this study. Here $N_{\rm conf}$ indicates the number of thermalised configurations used in the averages, am is the bare fermion mass in units of the lattice spacing a and the first column is a reference name for the set. Also indicated for each set is the lattice volume. Ensembles marked with $*$ do not meet the condition $Lam_{2^+} \gtrsim 9$, which was found to be a necessary prerequisite in order to have results free from finite-volume artefacts (see Sect. III D for details), and hence have not been used in our analysis.

Name	Volume	$-am$	$N_{\rm conf}$	Excluded
A1	16×8^3	1.475	1500	$*$
A2	16×8^3	1.500	1500	$*$
A3	16×8^3	1.510	1500	$*$
A4	16×8^3	1.510	4000	$*$
B1	24×12^3	1.475	1500	
B2	24×12^3	1.500	1500	
B3	24×12^3	1.510	4000	
C1	32×16^3	1.475	1500	
C2	32×16^3	1.490	1500	
C3	32×16^3	1.510	1500	
C4	32×16^3	1.510	4000	
C5	32×16^3	1.514	1500	
C6	32×16^3	1.519	1500	
C7	32×16^3	1.523	1500	$*$
D1	48×24^3	1.510	1534	
D2	48×24^3	1.523	2168	

ally the mass should be as small as possible. However, at fixed β and lattice size, strong lattice artefacts and finite size effects appear when the mass is reduced towards the chiral limit. Hence, the minimum mass that can be simulated depends on β and on the lattice volume V. When choosing simulation parameters, a compromise between the ideally suited situation and the emergence of practical difficulties needs to be reached, verifying *a posteriori* that the choice of parameters is meaningful for describing the physical system. Based on the obtained phase diagram and on the above considerations, a single value of the lattice spacing, set by $\beta = 2.05$, was chosen, and bare fermion masses were considered in the range $-1.523 \leq am \leq -1.475$. For the quantitative measurements that follow, lattice sizes of $N_T \times N^3$ between 16×8^3 and 48×24^3 were considered. Lattice volumes and other parameters are shown in Tab. II.

B. Centre symmetry

At zero temperature and infinite spatial volume, SU(N) gauge theories with adjoint fermions preserve the $(\mathbb{Z}(N))^4$ symmetry related to centre transformations in the four Euclidean directions. When shrinking the volume or increasing the temperature (the two mechanisms

TABLE III: Glueball masses and string tension

Name	$a\sqrt{\sigma}$	am_{0^+}	am_{2^+}
A1	0.424(13)	0.8422 ± 0.0968	1.3148 ± 0.2305
A2	0.335(10)	0.7320 ± 0.0885	1.4678 ± 0.2176
A3	0.299(12)	0.5690 ± 0.0585	1.6921 ± 0.3196
A4	—	0.5873 ± 0.0553	—
B1	0.378(19)	0.9582 ± 0.1174	1.8059 ± 0.3643
B2	—	0.7296 ± 0.1092	—
B3	0.322(10)	0.5284 ± 0.1494	—
C1	0.436(60)	0.9654 ± 0.1057	1.7461 ± 0.3526
C2	0.379(44)	0.8265 ± 0.0644	1.9130 ± 0.5004
C3	0.318(11)	0.5985 ± 0.0573	1.6285 ± 0.3079
C4	—	0.5901 ± 0.0438	—
C5	0.322(13)	0.5530 ± 0.0415	1.5834 ± 0.2263
C6	0.2859(75)	0.3689 ± 0.0437	1.9897 ± 0.2589
C7	0.2368(84)	0.3146 ± 0.0278	1.0188 ± 0.0977
D1	—	0.4609 ± 0.0553	—
D2	0.2354(56)	0.3355 ± 0.0264	1.3387 ± 0.1104

TABLE IV: PCAC and baryon masses (triplet channels).

Name	$am_{\rm PCAC}$	$am_{\rm pseudoscalar}$	$am_{\rm scalar}$	$am_{\rm vector}$
A1	0.1486(17)	—	0.9704(58)	—
A2	0.1108(20)	—	0.8432(81)	—
A3	0.0906(27)	—	0.763(12)	—
A4	0.0872(22)	—	0.747(10)	—
B1	0.1493(29)	—	0.9733(23)	2.297(59)
B2	0.1113(8)	1.969(39)	0.8449(31)	2.062(41)
B3	0.0911(7)	1.635(45)	0.7644(30)	—
C1	0.1490(3)	—	0.9723(12)	—
C2	0.1278(3)	—	0.9035(16)	—
C3	0.0911(3)	—	0.7646(15)	—
C4	0.0905(5)	1.594(58)	0.7645(17)	—
C5	0.0829(6)	1.712(31)	0.7288(29)	1.702(70)
C6	0.0659(9)	1.518(42)	0.6473(44)	—
C7	0.0484(5)	—	0.5480(36)	—
D1	0.0913(2)	—	0.7651(11)	—
D2	0.0472(3)	1.282(62)	0.5412(25)	—

TABLE V: Meson and spin-$\frac{1}{2}$ state masses (singlet channels).

Name	$am_{1/2}$	$am_{\rm scalar}$	$am_{\rm pseudoscalar}$	$am_{\rm vector}$	$am_{\rm axial}$
B1	1.707(20)	0.64(20)	0.9859(91)	1.1605(12)	2.27(67)
B2	1.535(72)	0.91(33)	0.839(45)	1.0504(23)	1.91(10)
B3	1.349(51)	0.53(11)	0.819(22)	0.9792(55)	—
C4	1.325(24)	0.602(85)	0.751(19)	0.9757(54)	2.260(47)
C5	1.284(22)	0.434(78)	0.750(17)	0.9433(34)	—
C6	1.200(73)	0.339(86)	0.741(38)	0.8635(48)	2.190(52)
D1	—	—	—	0.9761(53)	—
D2	0.949(34)	0.328(49)	0.598(33)	0.737(18)	1.664(76)

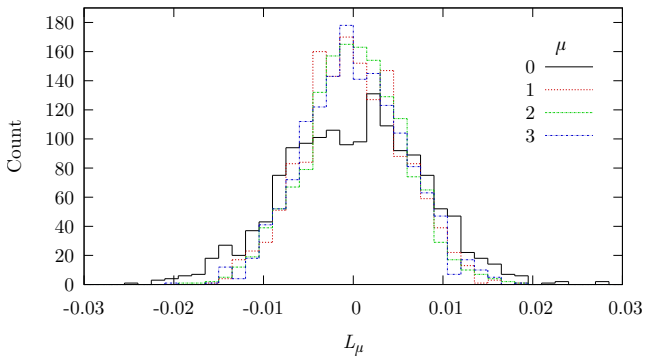

(a) C6

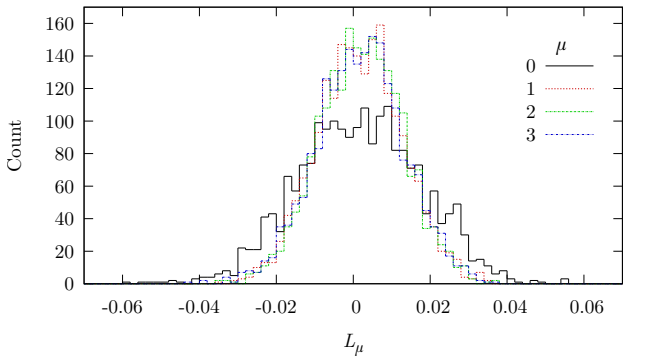

(b) D1

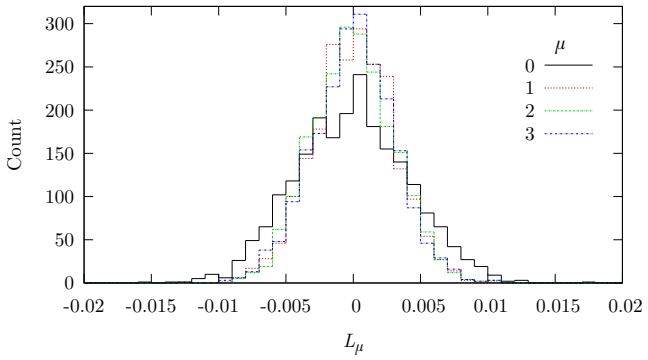

(c) D2

FIG. 2: (Color online) The histogram of the average Polyakov loop for all configurations belonging to the set shown in the label of each subfigure, for all space-time directions. The single peaks indicate an unbroken centre symmetry.

being connected in an Euclidean setup[6]), the system can pass through various phases (or more precisely regimes, if the number of degrees of freedom is finite) with different centre symmetry patterns [42].

The order parameter for the centre symmetry factor associated to the direction $\hat{\mu}$ is the vacuum expectation value $\langle L_\mu \rangle$ of the traced Polyakov loop in that direction

$$L_\mu = \sum_{i_\perp} \mathrm{Tr} \left(\prod_{i=0}^{N_\mu} U_\mu(x_\perp, x_\mu) \right) , \tag{33}$$

where x_μ is the μ-th coordinate, $x_\perp$ the set of coordinates in the perpendicular directions to $\hat{\mu}$ and N_μ the number of lattice points in the $\hat{\mu}$ direction.

The Polyakov loop can be used to detect finite volume artefacts. On a sufficiently large lattice, the distribution of the vacuum expectation values of all four Polyakov loops are symmetric with a peak at zero. A change of regime will occur when, as reducing the lattice size, N peaks will start to appear in one of the Polyakov loop distributions. As the lattice size is further reduced, the Polyakov loops show a more complicated pattern characterised by the distribution of one or more of them having N peaks. Finally, in the zero-volume limit, all the four Polyakov loop distributions are again peaked at zero [42]. Following the order of the discussion above, the regime connected with the infinite volume limit is the first of the two regimes characterised by a maximum of the Polyakov loop histogram at zero. In order to disentangle this from the opposite zero-volume limit, the Polyakov loop average needs to be investigated as a function of the lattice size.

The regime of our ensembles with respect to the $(\mathbb{Z}(2))^4$ symmetry was tested by investigation of averages of Polyakov loops. When finite size effects are absent, we expect the average of traced Polyakov loops in all directions to be consistent with zero within errors, with the histogram of values having a single peak at zero and being symmetric around that value. Polyakov loop averages with a doubly-peaked distribution at two non-zero values symmetric around the origin signal finite size effects [16]. Representative plots of $\langle L_\mu \rangle$ showing a distribution peaked in zero are given in Fig. 2. All the results reported here have been obtained for choices of parameters for which the system is in a regime with all the distributions of Polyakov loops peaked at zero. In order to check that this is the regime of the thermodynamic limit, we have observed that reducing the lattice size below a certain value gives rise to a two peak structure developing in the Polyakov loop distributions. This study indicates that our simulations are free from centre-related finite size artefacts.

[6] As in our simulations, we have assumed periodic boundary conditions for the gauge fields in all directions, periodic boundary conditions for fermionic fields in spatial directions and antiperiodic boundary conditions for fermionic fields in the temporal direction, the latter being related to the finite temperature setup.

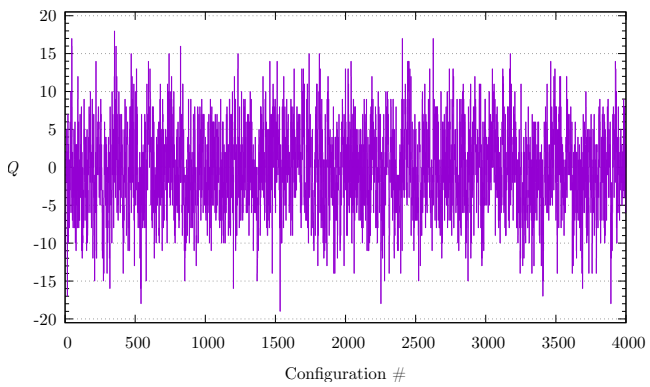

(a) C1

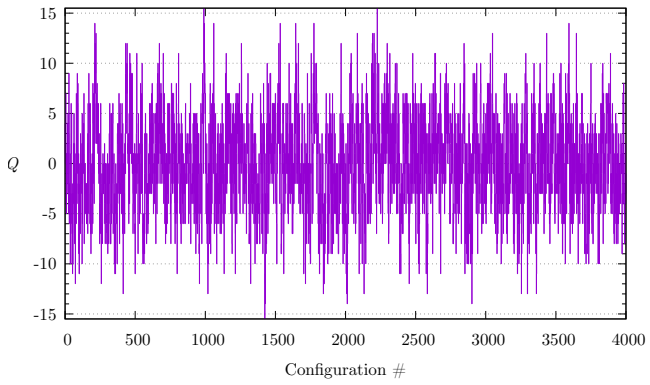

(b) C4

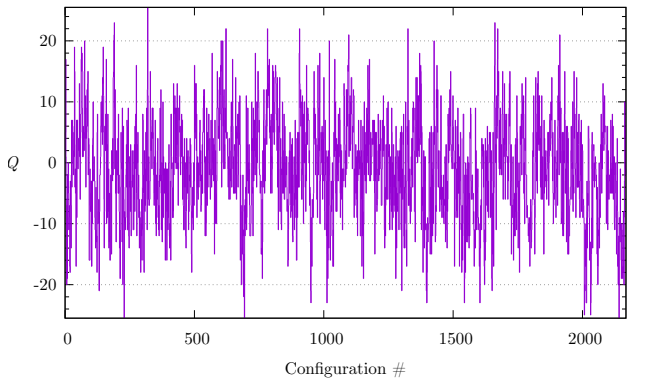

(c) D2

FIG. 3: (Color online) The history of the topological charge Q for the indicated ensembles; other ensembles had similar properties.

C. Topological charge

A potential problem of lattice simulations of gauge theories is the emergence of long autocorrelations among topological sectors at couplings that are crucial for taking the continuum limit. In order to understand whether this also happens in our case, we have monitored the topological charge history of our runs.

The topological charge of a lattice configuration can be defined as

$$Q = \frac{1}{32\pi^2} \sum_i \epsilon_{\mu\nu\rho\sigma} \mathrm{Tr}\left(U_{\mu\nu}(i) U_{\rho\sigma}(i)\right) \ , \qquad (34)$$

where the sum extends over the whole lattice, $\epsilon_{\mu\nu\rho\sigma}$ is the fully antisymmetric tensor and $U_{\mu\nu}(i)$ is the plaquette starting from point $i \equiv (\vec{x}, t)$ in direction $\hat{\mu}$ and coming back to i from $i + \hat{\nu}$. In the continuum limit, Q is an integer labelling the topological sector to which the configuration belongs.

Monte Carlo determinations of Q are hindered by ultraviolet fluctuations, which hide the underlying topological structure. These fluctuations can be removed using smoothing techniques such as cooling [43] or the more recently introduced Wilson flow [44], which are expected to provide similar benefits [45].

In an ergodic simulation, the system should efficiently explore topological sectors. However, long autocorrelations are shown to appear when the continuum limit is approached. These autocorrelations determine an increase of the required number of configurations that are needed to obtain statistically significant vacuum expectation values of physical observables. A recent description of the problem for QCD (and a proposed solution) can be found in [46]. Similar autocorrelations have been observed in investigations of novel strong dynamics beyond the standard model (see e.g. [47]).

We have measured the value of the topological charge for our configurations using equation (34). The ultraviolet fluctuations were filtered out using the cooling method described in [43, 48, 49]. Representative sample histories of Q are shown in Fig. 3. In general, the results were found to show good tunnelling behaviour, confirming that the Monte Carlo was not trapped in a single topological sector and supporting the robustness of our error estimates. A more technical discussion of instanton-related observables in our simulations (including the topological susceptibility and the correlation time of the topological charge) is provided in Appendix D.

Another check of finite size artefacts is provided by a study of the instanton size distribution [49]. For our choice of parameters, the instanton size distributions are those expected in the large volume limit. This investigation provides another indication that our simulations are free from the most obvious finite size artefacts.

D. Spectral observables

For the spectroscopic study, we considered masses of mesonic and baryonic two-fermion states, the 0^+ glueball (the 2^+ was also considered, but found to be too noisy to provide useful information), and a spin-$\frac{1}{2}$ state, as well as the fundamental string tension extracted using correlators of Polyakov loops (see e.g. [16]). Baryonic observables were calculated using two codes: one (HiRep) working in the Dirac basis and using stochastic

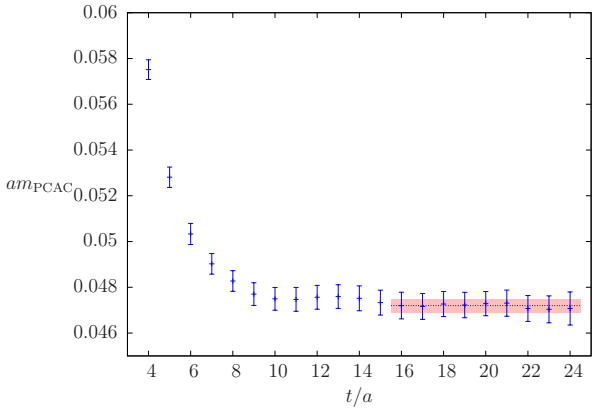

(a) PCAC.

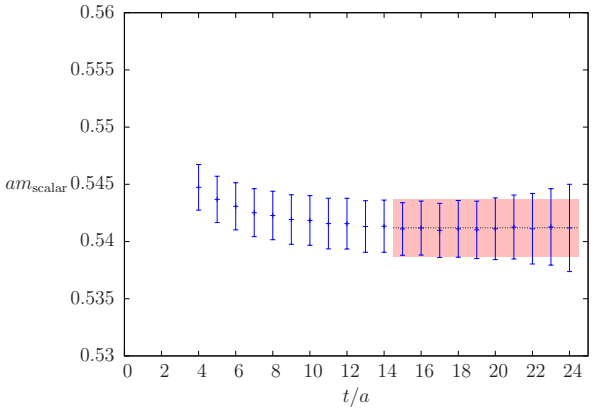

(b) 2^+ scalar baryon.

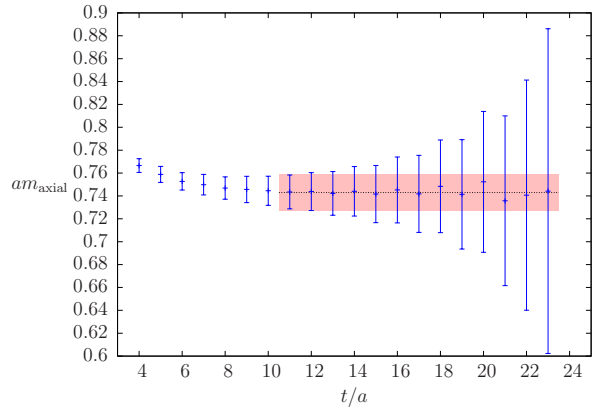

(c) 0^- axial vector meson.

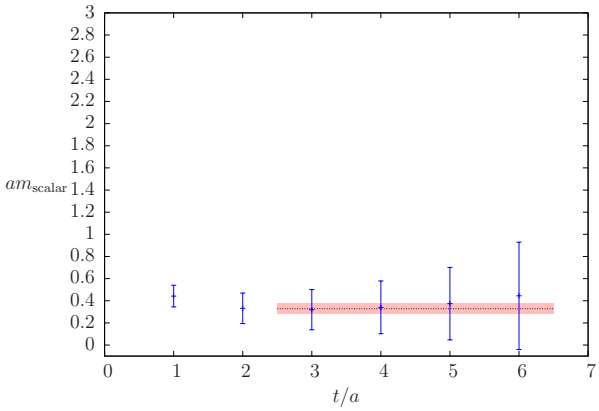

(d) 0^+ scalar meson.

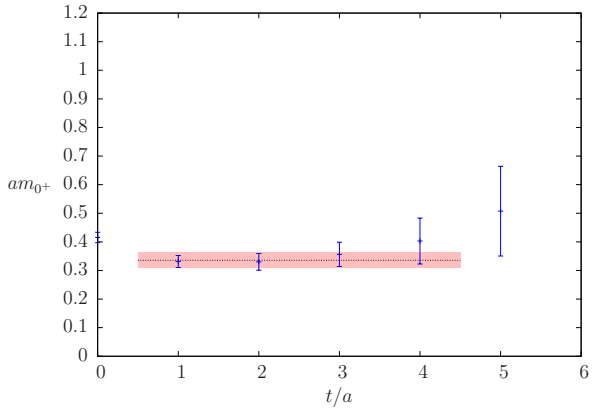

(e) 0^+ scalar glueball.

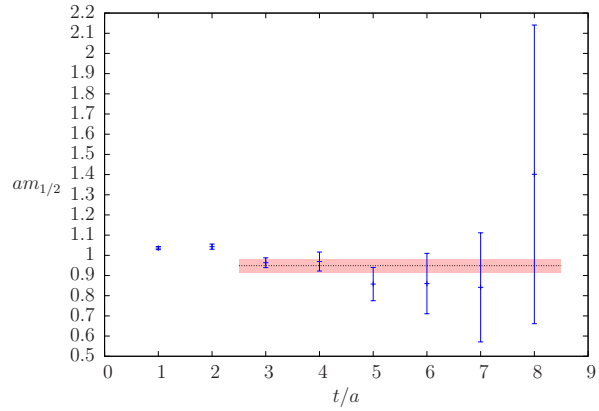

(f) spin-$\frac{1}{2}$ state.

FIG. 4: (Color online) Effective masses for the given states as a function of t in lattice units on the D2 ensemble. A fit of the plateau is also displayed, together with the fit range.

sources in color space (the Z2SEMWall method of [50]), and one developed for lattice studies of Super Yang–Mills theories [36]. Mesonic observables were calculated using the latter code. For the disconnected contributions the noisy estimator technique has been applied in combination with the truncated solver method [51]. This rather time consuming measurement has been carried out only on every 4th configuration. There is a significant difference in the relevance of the disconnected contribution for the different operators: it is the dominant part of

the scalar meson correlator, but negligible for the pseudoscalar meson. Gluonic observables were calculated using the methods described in [16, 41]. The spin-$\frac{1}{2}$ state is constructed in the continuum from the operator

$$O_{\text{spin-}\frac{1}{2}} = \sum_{\mu,\nu} \sigma_{\mu\nu} \text{tr}[F^{\mu\nu}\xi] \ , \tag{35}$$

where $\sigma_{\mu\nu} = \frac{1}{2}[\gamma_\mu, \gamma_\nu]$. This state, which can be seen as a bound state of a fermion and a gluon, has been measured using a combination of APE and Jacobi smearing, with the used tools described in [36].

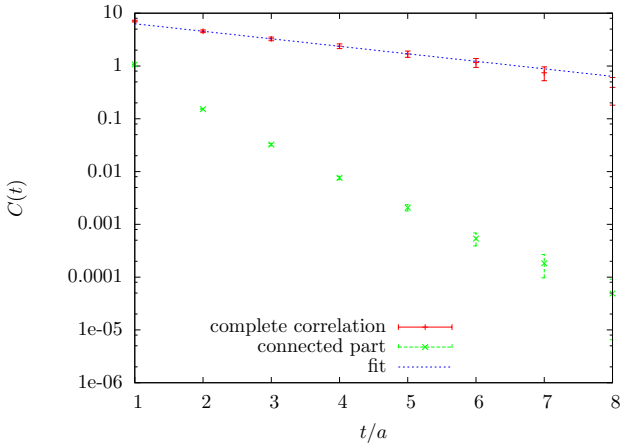

FIG. 5: (Color online) The connected correlator and the full correlator (which includes both connected and disconnected contributions) in the scalar meson channel for the ensamble D2.

A representative set of effective mass plots are shown in Figure 4 for the D2 ensamble. The errors on both the effective masses and the final fit were calculated using a blocked bootstrap method. At higher m_{PCAC} the quality of the the plateaux is comparable to those shown in Figure 4. In the panes of this figure, the bands show the extracted mass, and stretches across the data we have used for the fits. As expected, the highest quality plateaux are

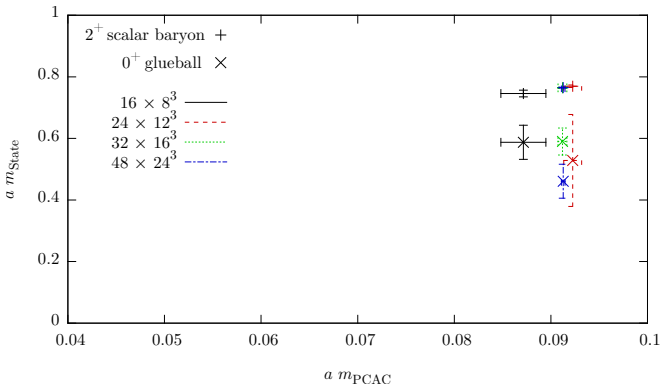

FIG. 6: (Color online) The 2^+ scalar baryon and 0^+ glueball masses, at $am = -1.51$, for the four lattice sizes considered.

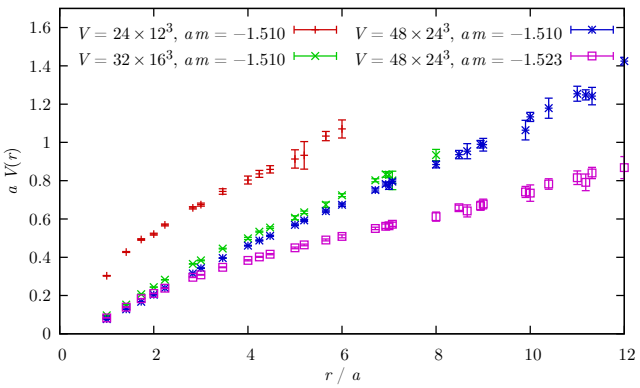

FIG. 7: (Color online) The static fermion potential of four selected lattices.

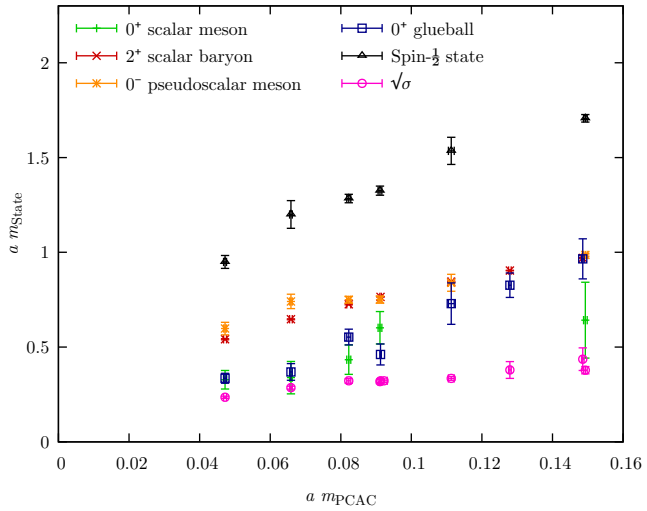

FIG. 8: (Color online) Selected spectrum of the theory, showing meson, baryon, glueball, and spin-$\frac{1}{2}$ states, and $\sigma^{1/2}$.

obtained for the PCAC mass and the scalar baryon. The quality is also good for the axial vector. Mass plateaux for the scalar meson, the scalar glueball and the spin-$\frac{1}{2}$ are limited to about four points. This is usual for those states. An analysis of the results suggests that the systematics associated with these latter plateaux should not affect the discussion provided in this paper. The relative contribution of the connected and the disconnected part to the scalar meson correlator for the set D2 is displayed in Fig. 5. The plot shows that the error is dominated by the disconnected contribution, which is neverthless computed with enough accuracy to provide a meaningful determination of the mass.

To probe the extent of possible finite-size effects, studies of the pseudoscalar and of the scalar mass (extracted in the gluonic channel) were made at $am = -1.51$ at each of the four lattices considered. As is shown in Fig. 6, the results on the three largest lattices were all found to agree, while the results on the smallest lattice (of volume

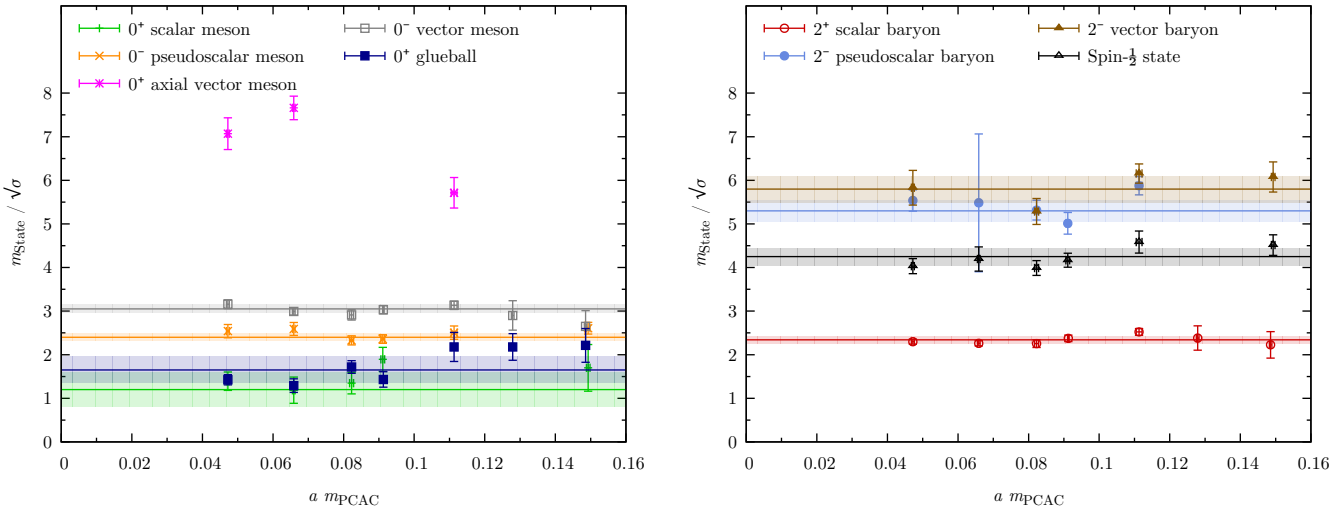

(a) Mesons and the 0^+ glueball.

(b) Baryons and the spin-$\frac{1}{2}$ state.

FIG. 9: (Color online) Spectrum of the theory, showing meson, glueball, and spin-$\frac{1}{2}$ states, all normalized by $\sigma^{1/2}$.

$V = T \times L^3 = 16 \times 8^3$) are inconsistent with the others. This result can be used to provide an estimate of the minimal box size needed to be free from finite size effects. Using the value of the string tension measured on the set of configurations at $am = -1.51$, we obtain the requirement $La\sqrt{\sigma} \geq 3.8$, or equivalently, in terms of the mass of the 2^+ baryon, $Lam_{2^+} \gtrsim 9$. The lattice sizes that do not respect this bound (and have therefore been excluded from our analysis) are marked with a $*$ in Tab. II. We also note that this bound has been obtained in the parameter region in which physical states are heavier in lattice units. Ideally, one would like to determine this bound for lower masses. This investigation is deferred to a future study.

As a cross-check of the determination obtained from Polyakov loop correlators, the string tension has been computed also using Wilson loops. The technicalities of this calculation are described in [16]. Some examples of the static inter-fermion potential from Wilson loops are shown in Fig. 7. The string tension has been extracted using the Cornell ansatz for the potential. The results found agree with the determination obtained using Polyakov loop correlators, but are in general less accurate. For this reason, in this section we have used the determination obtained from Polyakov loops.

The spectrum of the theory in lattice units (reported in Tabs. III, IV and V) is shown in Fig. 8, with Fig. 9 displaying ratios of masses over the string tension vs. $m_{\rm PCAC}$. In these plots, we show only results obtained on the largest available lattice at any simulated bare mass. Some states have proven to be numerically hard to measure, giving large error bars; for the sake of clarity, those states have been omitted from the figures. The size of the statistical error for the displayed states is affected by the autocorrelation time of the configurations (see appendix D), the statistics of the simulations and the quality of the corresponding mass plateau, and as a consequence presents some expected variation among states at fixed $m_{\rm PCAC}$ and for the same state across different values of $m_{\rm PCAC}$.

In an infrared conformal theory, the behaviour of the mass spectrum as a function of the quark mass is remarkably different than in a confining theory. In particular, the spectral signature of infrared conformality has been investigated in detail in [11, 15, 16, 52–54]. The conclusion from these works is that, unlike in QCD, in infrared conformal theories near the massless limit ratios of spectral masses stay constant as a function of the fermion mass. This implies that, as expected, there is no Goldstone boson associated to spontaneous breaking of chiral symmetry. Hence, considering mass ratios involving the would-be Goldstone boson of chiral symmetry breaking and studying their behaviour in the massless limit is a clear signal that distinguish spontaneous breaking of chiral symmetry and infrared (near-)concormality. In our case, from the data one can see that while all masses decrease monotonically as $m_{\rm PCAC} \to 0$, the ratio of spectral quantities to the string tension remains roughly constant for most quantities in the range studied[7], with some

[7] Although this behaviour is by itself a robust indication that the small mass regime of a near-conformal theory has been reached in our simulations, precision measurements of masses of bound states at zero fermion mass still require an extrapolation over a wide $m_{\rm PCAC}$ region. We remark that after performing a simple extrapolation to zero $m_{\rm PCAC}$ of our data, most of the quantities discussed in this section are compatible with zero in the chiral

(particularly the scalar glueball) showing some deviation (albeit within two standard deviations) at large fermion mass. Similar behaviour is observed for the 0^+ meson mass, which is compatible with the mass of the scalar glueball. A straightforward interpretation of the degeneracy found between the lowest-lying states in these two channels is that the glueball set of operators and the meson operator with 0^+ quantum numbers project onto the same ground state. This provides support for mixing between the scalar meson and the scalar glueball.

We also note that this scalar state is the lightest state in the spectrum. After having been observed in [11] in the SU(2) gauge theory with two adjoint fermions, the presence of a light scalar has proved to be a feature that keeps recurring in gauge theories near the conformal window (see [26, 55, 56] for recent lattice investigations and [57] for an approach based on gauge-string duality). The light scalar, which might be a signature in this class of models, is suggestive of a light Higgs appearing in this framework. This result indicates that strongly interacting dynamics beyond the standard model is not incompatible with the experimental constraint that the Higgs must be light in any extension of the standard model.

E. Chiral condensate anomalous dimension

The flatness of ratios of spectral quantities in this theory as the fermion mass is send to zero are suggestive of the model being in a conformal or near-conformal phase [11, 15, 16]. This indication is reinforced by the fact that the scalar is the lightest state in the theory. We stress that at the current stage of our investigations numerical evidence should be taken only as a hint. With this in mind, a conventional chirally broken phase seems to be excluded[8]. For this reason, for the purpose of understanding quantitatively the character of the theory, we will use a conformal ansatz and hence disregard chiral perturbation theory as a possible explanation of our model. This choice is based on the observation that in chiral perturbation theory the lightest degree of freedom is to be found in the 2^+ baryon channel. Hence, even if the system exhibited chiral symmetry breaking, our data would not be in the asymptotic regime, with the consequence that chiral perturbation theory is not applicable in this range of masses. Note that similar considerations also hold if one would include the light scalar in the effective lagrangian as done in [58], the 2^+ baryon still being the only degree of freedom surving in the deep infrared.

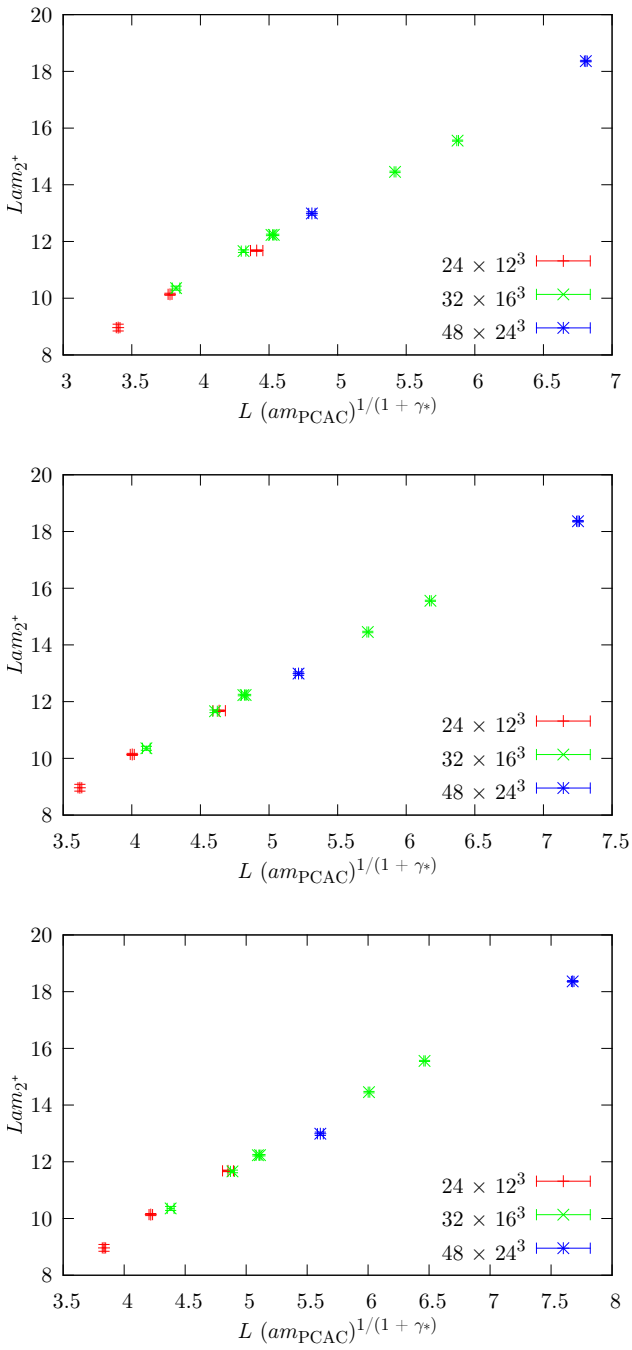

FIG. 10: (Color online) Plots of Lam_{2^+} as a function of $Lam_{\rm PCAC}^{1/(1+\gamma_*)}$ for the three lattice volumes 24×12^3, 32×16^3 and 48×24^3 and $\gamma_* = 0.9,\ 1.0,\ 1.1$ (top: $\gamma_* = 0.9$; middle: $\gamma_* = 1.0$; bottom: $\gamma^* = 1.1$). The results appear to identify a universal curve for $\gamma_* = 0.9 - 1.0$.

Near-conformality can be exploited to determine the value of the anomalous dimension of the chiral condensate γ_*. We may use various techniques to extract γ_*. We have used two methods for this work: finite-size

limit. Establishing if all, some, or none of these spectral quantities are zero in the zero-mass limit is of crucial importance for a definite answer to the questions we are addressing. However, this would require more extensive studies on larger lattices, which are outside the scope of this work.

[8] As we will remark in greater detail in the following section, the data are also compatible with a *walking* behaviour, i.e. a phase that at intermediate energies look infrared conformal, but at lower energies is in fact chirally breaking.

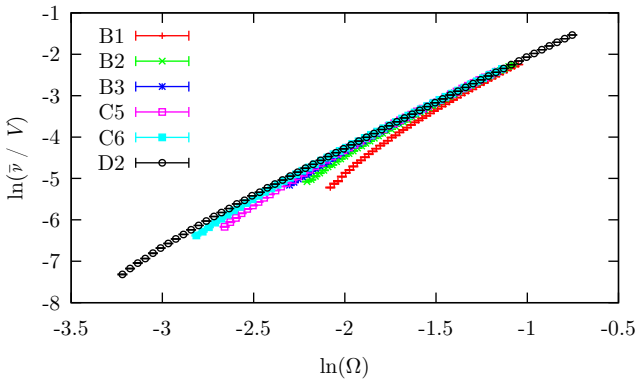

FIG. 11: (Color online) The behaviour of the Dirac mode number for a subset of the lattices considered.

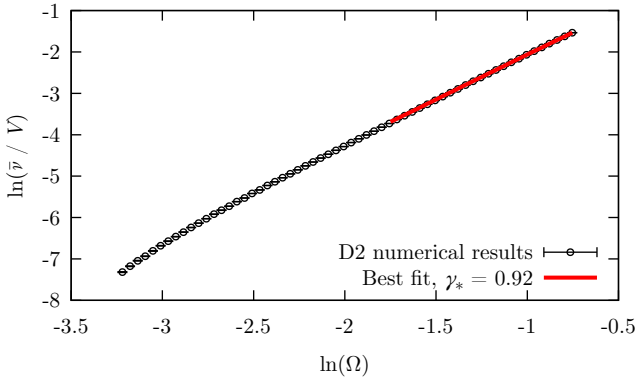

FIG. 12: (Color online) The behaviour of the Dirac mode number on the D2 lattice, compared with the results of the numerical fit, with $\gamma_* = 0.92$.

scaling predictions and scaling of the spectrum of the Wilson Dirac operator. For the first case, for a conformal theory, as a function of the $m_{\rm PCAC}$ mass, a spectral quantity $m_{\rm X}$ of the system follows the scaling relation [15, 16, 53, 54, 59–61]

$$Lam_{\rm X} = f\left(L\left(am_{\rm PCAC}\right)^{\frac{1}{1+\gamma_*}}\right) \ , \qquad (36)$$

for some function f, where $L \to \infty$ is the finite spatial extent of the lattice, and the combination $Lm_{\rm PCAC}^{1/(1+\gamma_*)}$ is kept constant. If the system is in the scaling region, then this relation may be used to estimate γ_* in the following way.

Firstly, we plot $Lam_{\rm X}$ against $L\left(am_{\rm PCAC}\right)^{1/(1+\gamma_*)}$ for all available lattice volumes on one plot for each of various values of γ_*. We then take the set of plots and find the region of γ_* that allows the sets from different lattices to lie on a single universal curve. In Fig. 10 we see the 2^+ scalar baryon analysed in this manner, at three values of γ_*; we see the best fit is observed in $0.9 \leq \gamma_0 \leq 1.0$, and so we expect the anomalous dimension to lie in this region[9].

A more precise method of determining γ_* is to fit the Dirac mode number $\overline{\nu}(\Omega)$ as a function of the Dirac eigenvalue Ω [62] (see also [63]). We expect the mode number to scale as:

$$a^{-4}\overline{\nu}(\Omega) \approx a^{-4}\overline{\nu}_0(M) + A[(a\Omega)^2 - (aM)^2]^{\frac{2}{1+\gamma_*}} \ , \qquad (37)$$

where $M = Z_A m_{\rm PCAC}$ and Z_A is the renormalisation constant of the isovector axial current (for further details, see [62]). The raw output of a set of simulations is plotted in Fig. 11.

In numerical studies of a mode number distribution that follows this relation, we have four parameters to fit for: $\overline{\nu}_0(M)$, A, $(aM)^2$, and γ_*. Additionally, in the presence of chiral symmetry, we would expect this relation to hold for $\Omega \to 0$; however, since simulations are performed at finite fermion mass, scaling is only seen in an intermediate range of Ω, which is not known *a priori*. This means that in addition to fitting for the four variables above, we must also carefully locate the scaling window of Ω. We choose to perform this analysis on the D2 lattice only, since the longer extent will provide the greatest opportunity to observe the scaling region. The corresponding data are plotted in Fig. 12.

To do this, we consider each possible window $[\Omega_{\rm LE}, \Omega_{\rm UE}]$ in turn, and perform an initial fit using two algorithms, Levenberg–Marquadt and simulated annealing, with $M = 0$ set to allow a convergent fit. To obtain an estimate of the stability of the fit, these initial values are then fed back into the same fitting algorithm a large number of times, with some random "jitter" applied, and bootstrap sampling is used to estimate the error on the average outputs.

From this, a set of plots can be drawn for each variable showing the value and error for all possible windows. Regions of stability in each variable can be seen as plateaux, and the scaling region is identified as the region that is most stable on all four plots simultaneously. This analysis (limited to a subset of $\Omega_{\rm LE}$, $\Omega_{\rm UE}$ for the sake of readability) for the Levenberg–Marquadt results on the D2 lattice is shown in Fig. 13, where γ_* was consistently found to lie in the range $0.9 \lesssim \gamma_* \lesssim 0.95$, with a best fit of $\gamma_* = 0.92(1)$, in agreement with the analysis based on the finite size scaling of m_{0^-}. The quality of the best fit is shown in Fig. 12. The simulated annealing results were found to be in good agreement with these data, and the best fit is consistent with the range found via the spectral scaling relations. Similar results have been obtained on other configuration sets. Putting together the more precise Dirac operator eigenvalue and the more qualitative spectral scaling determination, a safe estimate for γ_* is $\gamma_* = 0.925(25)$, with the central value that privileges the

[9] While a similar analysis on other states give compatible results, the 2^+ baryon, being the most accurately determined state in the spectrum, allows us to perform a better determination of γ_*.

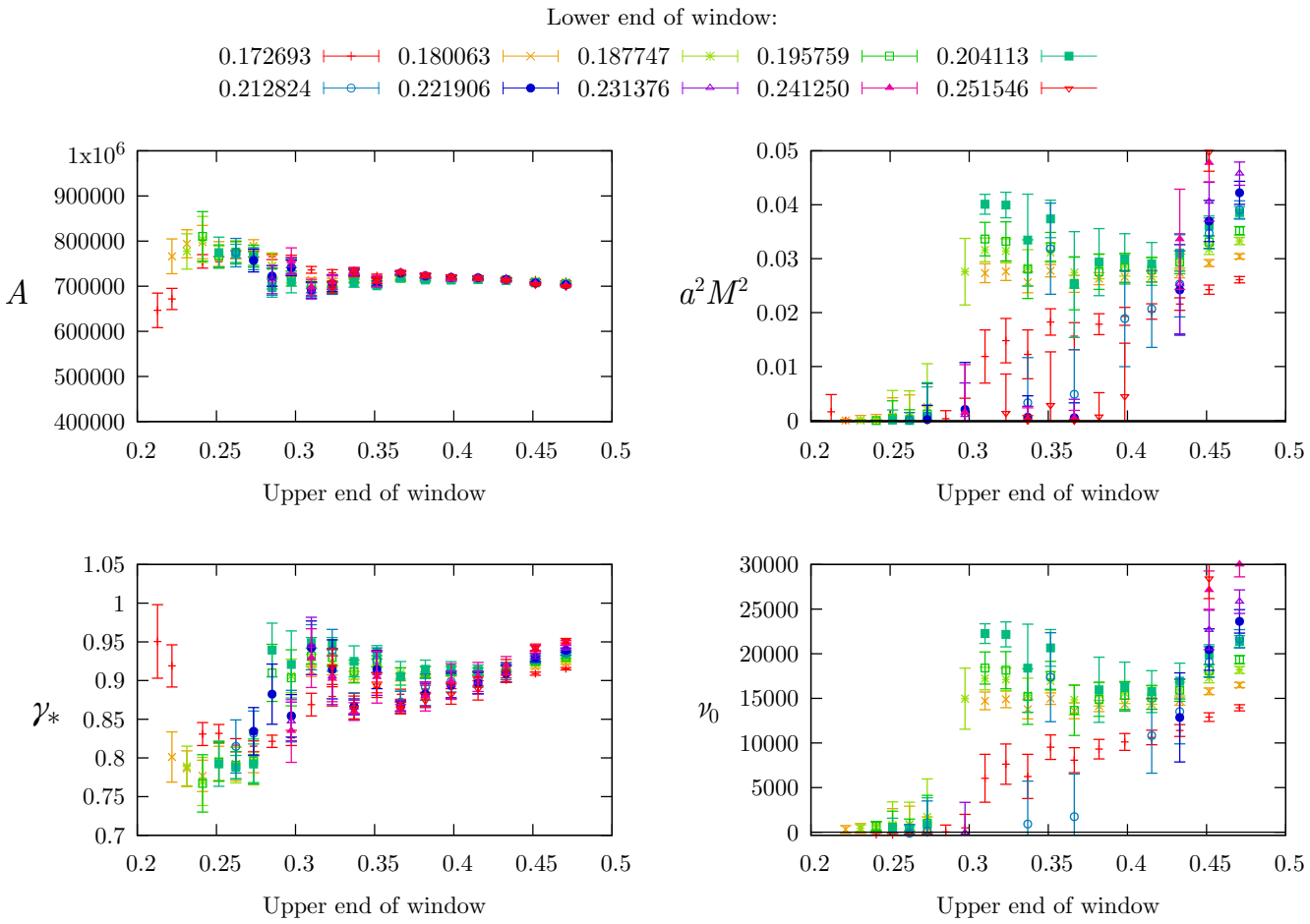

FIG. 13: (Color online) Plateaux for the fitted observables for the D2 data at various lengths and positions of the fitting window. The color represents the position of the lower end of the window, and the x-axis the upper end. The plateaux at the top-right of each plot were taken as the central values of our estimates.

result obtained with the former method and the error increased to be compatible within one standard deviation with the estimate coming from the finite-size scaling method. We note that this is the highest value found for the anomalous dimension in any lattice study of models relevant for strongly interacting dynamics beyond the standard model.

IV. DISCUSSION

Taken at face value, the numerical results of the previous section would imply infrared conformality of the theory with an anomalous dimension of order one. Since both the infrared conformality of the theory and the large anomalous dimension are somewhat unexpected, in this section we review arguments that seem to suggest a different result, discuss their extent of validity (and the extent of validity of our analysis) and outline where further simulations will help in pinning down potential remaining issues.

We have already stressed the large value of the anomalous dimension of the condensate, which makes this theory unique among those investigated on the lattice to date. However, we remark that the anomalous dimension has been obtained at a single lattice spacing, while the interesting quantity is its value in the continuum limit. In SU(3) with $N_{\rm f} = 12$ fundamental fermion flavours, a strong lattice spacing dependence of the anomalous dimension has been observed that can be successfully described by adding subleading corrections to the dominant scaling behaviour of observables near the infrared fixed point [64]. Hence, in order to determine the continuum value of the condensate anomalous dimension, a more extended investigation involving higher β values would be needed. Such an investigation will enable us to perform a robust extrapolation that includes scaling violations. In this work, we have used the standard Wilson action for the gauge fields and the Wilson discretisation of fermions. The expected discretisation errors can be reduced by using improved actions. In the absence of a more detailed study, we will make the working assumption that the value of the anomalous dimension will not change significantly when extrapolated to the continuum.

At a superficial sight, supporting cases for a non-conformal behaviour in the theory discussed in this pa-

per seem to come from arguments based on the two-loop β-function [65] and arguments based on the Seiberg and Witten solution of $\mathcal{N} = 2$ super Yang–Mills [29], which is related to our theory by an infinite mass deformation for the scalar. As noted in the introduction, the behaviour we have found does not generate any tension with the Seiberg and Witten result for $\mathcal{N} = 2$. In fact, the $\mathcal{N} = 2$ theory undergoes spontaneous symmetry breaking from gauge group SU(2) down to U(1) at any value of the Higgs condensate. When a small mass is given to the Higgs field, this moduli space is lifted and in the two resulting vacua monopoles condense, giving rise to Abelian confinement via the dual superconductor mechanism (already advocated before for QCD in [66]). A deformation retaining supersymmetry allows one to construct a path leading from $\mathcal{N} = 2$ to $\mathcal{N} = 1$ super Yang–Mills, with the latter theory confining. However, the deformation that takes $\mathcal{N} = 2$ super Yang–Mills to the gauge theory investigated in this work does not retain supersymmetry, and as such does not allow to argue about the phase of the theory we are interested in, starting from the original analytic result. It should also be stressed that the original $\mathcal{N} = 2$ super Yang–Mills theory lives in the Coulomb branch (i.e. the infrared limit is Abelian and conformal) and when deformed with a small mass term for the Higgs field the resulting theory has Abelian confinement of the electric charge, which is inherently different from the confinement observed in non-supersymmetric non-Abelian gauge theories [67]. In other words, this theory does not confine in the way a consistent argument would require. Hence, it can not be used as a starting point for arguing about confinement in the $N_{\rm f} = 1$ Dirac adjoint case.

Concerning the β-function argument, the underlying result is entirely based on perturbation theory, which is expected to break down when attempting a description of a strongly coupled infrared fixed point. This has been observed for SU(2) with two Dirac flavours in the adjoint representation, which was expected to be confining (albeit near the onset of the conformal window) perturbatively, but has been shown to be infrared conformal by lattice calculations.

Recently, it has been noticed in [68] (see also [69]) that there is an apparent tension between large-N volume reduction (which is expected to hold in theories with adjoint fermions) and presence of a Hagedorn-type density of states (which characterise confining theories). The authors advocate a solution based on an emerging fermionic symmetry at large N. However, on the light of our study, another possibility is that theories with $N_{\rm W}$ Weyl flavours are not confining when $N_{\rm W} > 1$, as there are indications for our case ($N_{\rm W} = 2$) and for the two adjoint Dirac flavour theory ($N_{\rm W} = 4$).

However, even if those arguments in favour of confining behaviour have possible breaches, it is still possible that our lattice simulations are in an intermediate mass regime and that at lower masses the model shows confining behaviour[10]. In order to check whether we can see this change in behaviour, we are performing simulations at larger volumes and lower masses. If the theory turns out to be confining in the deep infrared, the implication is that SU(2) with one adjoint fermion is walking, i.e. near-conformal in an intermediate energy range before turning confining at some low energy scale. This is the wanted behaviour for constructing a phenomenologically viable model of strongly interacting dynamics causing electroweak symmetry breaking, with the anomalous dimension being in the region of values compatible with experimental constraints.

Finally, our model only contains two Goldstone bosons associated with the chiral symmetry breaking, while phenomenologically at least three would be required to account for the standard model electroweak symmetry breaking. Nevertheless, the system studied here can be thought of as a sector of a richer theory containing also fermions in the fundamental representation, known as *ultraminimal technicolor*, whose phenomenology has been first explored in [70]. Our results suggest that a model constructed along the lines of ultraminimal technicolor could be compatible with phenomenology.

V. CONCLUSIONS

In this paper, we have performed a first numerical exploration of SU(2) gauge theory with one Dirac flavour. After investigating the phase structure of the theory, we have performed an extensive study at a value of the coupling that we have found to be continuously connected with the continuum limit of the theory. By studying the scaling of the spectrum and of the eigenvalues of the Dirac operator as the mass is reduced towards the chiral limit and the lattice is kept large enough for finite size artefacts to be under control, we have found indication of a conformal infrared behaviour with an anomalous dimension $0.9 \lesssim \gamma_* \lesssim 0.95$. If this features are confirmed by more extended simulations aimed at extrapolations to the continuum limit, the model will provide the first theory in the conformal window that has an anomalous dimension compatible with phenomenological constraints. Another possibility is that the theory is walking, and we are just observing its behaviour at intermediate energy scales. This case would also be interesting, as this would result in the first observation of a near-conformal

[10] We note that this is a logical possibility for any lattice simulation of this type, and the ability to observe in practice the true chiral behaviour in this case crucially depends on the separation between the two scales at which the plateau in the spectrum is observed. In particular, for phenomenology a large scale separation (of a few orders of magnitude) is required. Observing both regimes in a theory with such a large scale separation is a prohibitive task for lattice simulations, given the current techniques and the current computational resources.

theory with a large anomalous dimension. Such an observation would be again of theoretical relevance towards the construction of a phenomenologically viable explanation of electroweak symmetry breaking based on a novel strong dynamics beyond the standard model. Although the system studied here does not possess enough Goldstone bosons to provide a complete description of electroweak symmetry breaking due to a novel strong interaction, it might appear as a sector of a theory that could realise such a mechanism of electroweak symmetry breaking. Finally, we remark that the finding of a large anomalous dimension is relevant not only for understanding the viability of electroweak symmetry breaking by a new strong force, but also for advancing our understanding of the phase diagram of non-Abelian gauge theories.

Acknowledgments

We thank A. Patella for participating to the early stages of this project, for his suggestions and his critical reading of this manuscript. We would like to thank A. Cherman, T. DeGrand, M. Lombardo, E. Pallante, F. Sannino and M. Ünsal for discussions on various aspects of this project. BL is indebted with D. Dorigoni and T. Hollowood for enlightening discussions on $\mathcal{N} = 2$ Super Yang–Mills. Part of this work was performed when B.L. visited the Aspen Center for Physics (NSF Grant No. 1066293), which he thanks for hospitality. EB thanks the members of the LatKMI collaboration for helpful discussions and the Kobayashi–Maskawa Institute for hospitality during the latest stages of this work. Numerical computations were executed in part on the Blue Gene/P machine in Swansea University and the ULGQCD cluster in the University of Liverpool (part of the DiRAC facility supported by STFC), on the HPC Wales cluster in Cardiff, supported by the ERDF through the WEFO (part of the Welsh Government), on the BlueGene/Q system at the Hartree Centre (supported by STFC) and on the BlueGene/Q system at the University of Edinburgh (part of the DiRAC2 facility supported by STFC). This project has been supported by STFC (grant ST/G000506/1), and also by the JSPS Grant-in Aid for Scientific Research (Grant No. #23-01781 (EB)). EB is also partially supported by the JSPS Postdoctoral Fellowships for Foreign Researchers (PE13578).

Appendix A: Notations and conventions

In this Appendix, we describe for convenience the notations and the conventions on the Dirac algebra we have used for deriving the results of Sect. II.

In Minkowski space, with the metric tensor $g = \mathrm{diag}(+1, -1, -1, -1)$, we choose to use a chiral representation of the Dirac algebra, with

$$\gamma^\mu = \begin{pmatrix} 0 & \overline{\sigma}_\mu \\ \sigma_\mu & 0 \end{pmatrix} , \tag{A1}$$

where in turn

$$\sigma^\mu = (\mathbb{1}_2, \vec{\sigma}) , \quad \overline{\sigma}^\mu = (\mathbb{1}_2, -\vec{\sigma}) . \tag{A2}$$

$\vec{\sigma} = (\sigma_1, \sigma_2, \sigma_3)$ is the 3-vector formed from the Pauli matrices

$$\sigma_1 = \begin{pmatrix} 0 & 1 \\ 1 & 0 \end{pmatrix}, \sigma_2 = \begin{pmatrix} 0 & -i \\ i & 0 \end{pmatrix}, \sigma_3 = \begin{pmatrix} 1 & 0 \\ 0 & -1 \end{pmatrix} . \tag{A3}$$

and $\mathbb{1}_2$ is the 2×2 identity matrix. As usual, we define

$$\gamma_5 = i\gamma_0\gamma_1\gamma_2\gamma_3 = \begin{pmatrix} \mathbb{1}_2 & 0 \\ 0 & -\mathbb{1}_2 \end{pmatrix} . \tag{A4}$$

Charge conjugation is defined as

$$\psi_\mathrm{C} = C\overline{\psi}^\mathrm{T} \tag{A5}$$

where

$$C = i\gamma_0\gamma_2 = i \begin{pmatrix} \sigma_2 & 0 \\ 0 & -\sigma_2 \end{pmatrix} . \tag{A6}$$

The properties

$$C^\dagger = C^\mathrm{T} = -C , \tag{A7}$$

$$C\gamma_\mu C = \gamma_\mu^\mathrm{T} , \tag{A8}$$

$$C\gamma_5 C = -\gamma_5 . \tag{A9}$$

easily follow from the definition.

Appendix B: A note on states and parity

Our naming convention for bound states and lattice operators relevant for this investigation is different from the one used in lattice simulations of QCD and supersymmetric Yang–Mills theory. In order to clarify the correspondence, we discuss in this Appendix the relation between our classification of the spectrum and others found in the literature, in particular with connection to the mesonic and baryonic operators we are using. If one compares the states studied here to their QCD equivalents, or to other theories beyond the standard model, it is important to keep in mind the differences in the conventions we are going to expose.

In this work, fermion bilinears are meson and baryon operators. This is due to the fact that the gauge group (in our case, SU(2)) is (pseudo-)real. This is similar to the notion of baryons or diquarks in other investigations of SU(2) gauge theories with fermions in the fundamental representation (see e.g. [71] and references therein).

In the notation in terms of two Majorana fermions, all these states are referred to as mesons. In supersymmetric Yang–Mills theory a meson is named after its QCD equivalent, which is a flavour singlet meson. For instance, the scalar meson is called adjoint f_0 and the pseudoscalar meson adjoint η'.

In QCD the triplet γ_5 meson operator is related to the pion, the Goldstone boson of chiral symmetry breaking. This state becomes massless for vanishing $m_{\rm PCAC}$ and is the lowest state in the spectrum at small enough fermion mass. In several works related to theories different from QCD one adopts the convention to call pions the Goldstone bosons related to chiral symmetry breaking and define parity in such a way that these states are pseudoscalar. In investigations of supersymmetric Yang–Mills theory, for example, the chiral symmetry breaking pattern is defined in a partially quenched setup [35] and the light meson is called adjoint pion. Under the Lorentz group, the corresponding creation operator can be made to transform as a pseudoscalar if one deviates from the definition of the parity (13), which is the same as in QCD. A consequence of that definition is that Majorana flavours are mixed by a parity transformation:

$$\xi_+(t,\vec{x}) \mapsto i\gamma_0\xi_-(t,-\vec{x}) \ . \tag{B1}$$

If one uses instead

$$\psi(t,\vec{x}) \mapsto i\gamma_0\gamma_5\psi(t,-\vec{x}) \ , \tag{B2}$$

$$\overline{\psi}(t,\vec{x}) \mapsto -i\overline{\psi}(t,-\vec{x})\gamma_0\gamma_5 \ , \tag{B3}$$

the two Majorana flavours do not mix. With this choice, the parity quantum numbers of what in our conventions are the baryonic states are interchanged (pseudoscalar becomes scalar and vice versa). Hence what is called in other investigations a pseudoscalar meson and the (adjoint) pion, in our study is the scalar baryon. While the convention used elsewhere might seem more natural from the point of view of associating states to their QCD equivalent, ours treats on equal footing the left and right component of the Dirac spinor, as it happens for the standard definition of the parity in QCD. Ultimately, were the theory studied in this work to be found in nature, the interaction of its particles with the standard model particles would provide a natural way of fixing the arbitrariness in the definition of the parity.

Appendix C: Correlation functions of fermion bilinears

Our nomenclature for the contraction of correlation functions borrows from that of QCD for the sake of familiarity. Consider a correlation function for a theory with $N_{\rm f} \neq 1$,

$$I(x,y) = \frac{1}{Z}\int DUD\overline{\psi}D\psi\, \overline{\overline{\psi}_a\overline{\Gamma}\psi_b(x)\,\overline{\psi}_a\Gamma\psi_b(y)}e^{-S} \ , \tag{C1}$$

where a, b are flavour indices, to be contracted with Wick's theorem, and Z is the path integral. In the case $a \neq b$, then only the upper contraction gives a non-zero contribution, which then becomes a term of the form $-{\rm tr}\overline{\Gamma}D^{-1}(x;y)\Gamma D^{-1}(y;x)$, which we refer to as both the triplet (this name being inspired by the isospin symmetry of QCD) and the connected contribution (where the terminology refers to the fact that in terms of purely fermionic lines the corresponding diagram is connected). If $a = b$, however, both contractions can give non-zero contributions, resulting in a linear combination of the previous term and one of the form ${\rm tr}\overline{\Gamma}D^{-1}(x;x){\rm tr}\Gamma D^{-1}(y;y)$. The latter term we refer to as the disconnected contribution, while the linear combination we call the singlet. The reason why triplet correlation functions may give physically meaningful states in what is a 1-flavour theory (where one would naïvely assume $a = b$, so only singlets are valid) is discussed in the main body of the text.

Appendix D: Further technical details on lattice simulations

TABLE VI: Further details of the RHMC parameters used in this study. Shown are the molecular dynamics trajectory length $t_{\rm len}$, the length of the fermionic molecular dynamics substeps $n_{\rm steps}$, the number of pseudofermions $n_{\rm pf}$, and the average plaquette. The number of gauge substeps was fixed at $2n_{\rm steps}$.

Name	$t_{\rm len}$	$n_{\rm steps}$	$n_{\rm pf}$	Plaquette
A1	1.0	10	1	0.57848(27)
A2	1.0	10	1	0.58833(36)
A3	1.0	10	1	0.59263(30)
A4	1.0	10	2	0.59428(14)
B1	1.0	10	1	0.57819(25)
B2	1.0	10	1	0.58787(27)
B3	1.0	10	2	0.59291(11)
C1	1.0	20	1	0.57841(26)
C2	1.0	20	1	0.58336(27)
C3	1.0	20	1	0.59316(28)
C4	4.0	45	2	0.59388(3)
C5	1.0	20	1	0.59554(28)
C6	1.0	20	1	0.60020(3)
C7	1.0	20	1	0.60445(31)
D1	4.0	65	2	0.59358(2)
D2	1.0	40	1	0.60613(2)

In this appendix we give some "under-the-hood" details of the lattice simulations performed, for completeness. Table VI presents some variables from the RHMC. $t_{\rm len}$ is the length of the molecular dynamics trajectory. Different time substeps are used for the gauge and fermionic actions: for each (relatively expensive) fermion

TABLE VII: The average topological charge, topological susceptibility, and integrated autocorrelation time of the topological charge.

Name	$\langle Q \rangle$	χ_{top}	τ_Q
A1	−0.02(9)	$2.32(8) \times 10^{-4}$	4.6
A2	0.04(8)	$1.94(7) \times 10^{-4}$	3.7
A3	0.13(5)	$1.68(7) \times 10^{-4}$	2.3
A4	0.07(6)	$1.65(4) \times 10^{-4}$	6.2
B1	0.11(19)	$1.94(7) \times 10^{-4}$	4.2
B2	−0.01(16)	$1.87(7) \times 10^{-4}$	3.1
B3	0.12(15)	$1.58(3) \times 10^{-4}$	9.1
C1	−0.46(31)	$2.65(9) \times 10^{-4}$	3.3
C2	0.09(36)	$2.15(8) \times 10^{-4}$	5.0
C3	−0.54(26)	$1.64(7) \times 10^{-4}$	3.1
C4	−0.20(14)	$1.60(5) \times 10^{-4}$	1.3
C5	−0.42(24)	$1.51(6) \times 10^{-4}$	3.0
C6	−0.21(30)	$1.27(5) \times 10^{-4}$	5.9
C7	−0.01(35)	$1.05(4) \times 10^{-4}$	9.1
D1	−0.29(36)	$1.98(7) \times 10^{-4}$	1.3
D2	−1.39(49)	$1.20(4) \times 10^{-4}$	6.2

substep, two (cheaper) gauge substeps are used. This allows an increase in precision without significantly increasing the cost of computation. We show the substep length for the fermionic part; the gauge counterpart is a factor of two smaller. The RHMC algorithm makes use of an arbitrary number of pseudofermions N_{pf} in order to compute the fractional powers of the fermion matrix necessary to probe non-even N_{f}. As a minimum, $N_{\text{pf}} = N_{\text{f}}$; higher numbers of pseudofermions require more computational effort but increase the precision of the rational approximations performed by the algorithm. We made use of a higher number of pseudofermions in the finite-volume study to cross-check that using a single pseudofermion did not give inaccurate results. Finally, the average plaquette (normalized to unity) is quoted. For fuller details of the algorithm and definitions of all of these quantities, the interested reader is referred to [21]. The acceptance rate was held between 75% and 93%, while $dt = t_{\text{len}}/n_{\text{steps}}$ ranges from 0.025 to 0.1.

Table VII shows some topological observables. The average topological charge $\langle Q \rangle$ is consistent with zero within 2σ for all but two parameter sets (namely A3 and D2), indicating good ergodicity. A3 is ruled out from consideration anyway due to finite-volume effects, while looking at the time history of Q for D2 shows that adequate tunnelling is taking place for the ensemble to be considered ergodic. The topological susceptibility (calculated as $(\langle Q^2 \rangle - \langle Q \rangle^2)/V$), and the integrated autocorrelation time of Q, are also shown. When measured in terms of the autocorrelation time of Q, in the worse case we have around 165 independent blocks of configurations. This should provide enough statistics for an unbiased estimate of the observables discussed in this work.

[1] G. Aad et al. (ATLAS Collaboration), Phys.Lett. **B716**, 1 (2012), 1207.7214.
[2] S. Chatrchyan et al. (CMS Collaboration), Phys.Lett. **B716**, 30 (2012), 1207.7235.
[3] S. Weinberg, Phys.Rev. **D13**, 974 (1976).
[4] L. Susskind, Phys.Rev. **D20**, 2619 (1979).
[5] E. Eichten and K. D. Lane, Phys.Lett. **B90**, 125 (1980).
[6] B. Holdom, Phys.Rev. **D24**, 1441 (1981).
[7] B. Holdom, Phys.Lett. **B150**, 301 (1985).
[8] K. Yamawaki, M. Bando, and K.-i. Matumoto, Phys.Rev.Lett. **56**, 1335 (1986).
[9] T. W. Appelquist, D. Karabali, and L. Wijewardhana, Phys.Rev.Lett. **57**, 957 (1986).
[10] M. E. Peskin and T. Takeuchi, Phys.Rev. **D46**, 381 (1992).
[11] L. Del Debbio, B. Lucini, A. Patella, C. Pica, and A. Rago, Phys.Rev. **D80**, 074507 (2009), 0907.3896.
[12] A. J. Hietanen, K. Rummukainen, and K. Tuominen, Phys.Rev. **D80**, 094504 (2009), 0904.0864.
[13] S. Catterall, J. Giedt, F. Sannino, and J. Schneible (2009), 0910.4387.
[14] F. Bursa, L. Del Debbio, L. Keegan, C. Pica, and T. Pickup, Phys.Rev. **D81**, 014505 (2010), 0910.4535.
[15] L. Del Debbio, B. Lucini, A. Patella, C. Pica, and A. Rago, Phys.Rev. **D82**, 014509 (2010), 1004.3197.
[16] L. Del Debbio, B. Lucini, A. Patella, C. Pica, and A. Rago, Phys.Rev. **D82**, 014510 (2010), 1004.3206.
[17] F. Bursa, L. Del Debbio, D. Henty, E. Kerrane, B. Lucini, et al., Phys.Rev. **D84**, 034506 (2011), 1104.4301.
[18] S. Catterall, L. Del Debbio, J. Giedt, and L. Keegan, Phys.Rev. **D85**, 094501 (2012), 1108.3794.
[19] T. DeGrand, Y. Shamir, and B. Svetitsky, Phys.Rev. **D83**, 074507 (2011), 1102.2843.
[20] S. Catterall and F. Sannino, Phys.Rev. **D76**, 034504 (2007), 0705.1664.
[21] L. Del Debbio, A. Patella, and C. Pica, Phys.Rev. **D81**, 094503 (2010), 0805.2058.
[22] A. J. Hietanen, J. Rantaharju, K. Rummukainen, and K. Tuominen, JHEP **0905**, 025 (2009), 0812.1467.
[23] S. Catterall, J. Giedt, F. Sannino, and J. Schneible, JHEP **0811**, 009 (2008), 0807.0792.
[24] R. S. Chivukula and E. H. Simmons, Phys.Rev. **D82**, 033014 (2010), 1005.5727.
[25] L. Del Debbio, B. Lucini, C. Pica, A. Patella, A. Rago, et al. (2013), 1311.5597.
[26] Y. Aoki et al. (the LatKMI Collaboration) (2014), 1403.5000.
[27] J. Giedt, PoS **LATTICE2012**, 006 (2012).
[28] J. Kuti, PoS **LATTICE2013**, 004 (2013).
[29] N. Seiberg and E. Witten, Nucl.Phys. **B426**, 19 (1994), hep-th/9407087.
[30] A. Hietanen and R. Narayanan, Phys.Rev. **D86**, 085002 (2012), 1204.0331.
[31] B. Bringoltz, M. Koren, and S. R. Sharpe, PoS **LAT-**

TICE2012, 045 (2012), 1212.0535.
[32] A. González-Arroyo and M. Okawa (2013), 1311.3778.
[33] D. D. Dietrich and F. Sannino, Phys.Rev. **D75**, 085018 (2007), hep-ph/0611341.
[34] A. Athenodorou, E. Bennett, G. Bergner, B. Lucini, and A. Patella, PoS **LATTICE2013**, 066 (2013), 1311.4155.
[35] G. Münster and H. Stüwe, JHEP **1405**, 034 (2014), 1402.6616.
[36] G. Bergner, I. Montvay, G. Münster, U. D. Ozugurel, and D. Sandbrink, JHEP **1311**, 061 (2013), 1304.2168.
[37] M. Clark and A. Kennedy, Phys.Rev.Lett. **98**, 051601 (2007), hep-lat/0608015.
[38] L. Del Debbio, B. Lucini, A. Patella, and C. Pica, JHEP **0803**, 062 (2008), 0712.3036.
[39] I. Montvay, Nucl.Phys. **B466**, 259 (1996), hep-lat/9510042.
[40] A. Donini, M. Guagnelli, P. Hernandez, and A. Vladikas, Nucl.Phys. **B523**, 529 (1998), hep-lat/9710065.
[41] B. Lucini, A. Rago, and E. Rinaldi, JHEP **1008**, 119 (2010), 1007.3879.
[42] G. Cossu and M. D'Elia, JHEP **0907**, 048 (2009), 0904.1353.
[43] M. Teper, Phys.Lett. **B162**, 357 (1985).
[44] M. Luscher, JHEP **1008**, 071 (2010), 1006.4518.
[45] C. Bonati and M. D'Elia, Phys.Rev. **D89**, 105005 (2014), 1401.2441.
[46] M. Luscher and S. Schaefer, JHEP **1107**, 036 (2011), 1105.4749.
[47] Z. Fodor, K. Holland, J. Kuti, S. Mondal, D. Nogradi, et al., JHEP **1409**, 018 (2014), 1406.0827.
[48] D. A. Smith and M. J. Teper (UKQCD collaboration), Phys.Rev. **D58**, 014505 (1998), hep-lat/9801008.
[49] E. Bennett and B. Lucini, Eur.Phys.J. **C73**, 2426 (2013), 1209.5579.
[50] P. Boyle, A. Juttner, C. Kelly, and R. Kenway, JHEP **0808**, 086 (2008), 0804.1501.
[51] G. S. Bali, S. Collins, and A. Schafer, Comput.Phys.Commun. **181**, 1570 (2010), 0910.3970.
[52] V. Miransky, Phys.Rev. **D59**, 105003 (1999), hep-ph/9812350.
[53] B. Lucini, Phil.Trans.Roy.Soc.Lond. **A368**, 3657 (2010), 0911.0020.
[54] L. Del Debbio and R. Zwicky, Phys.Rev. **D82**, 014502 (2010), 1005.2371.
[55] Y. Aoki et al. (LatKMI Collaboration), Phys.Rev.Lett. **111**, 162001 (2013), 1305.6006.
[56] Z. Fodor, K. Holland, J. Kuti, D. Nogradi, and C. H. Wong, PoS **LATTICE2013**, 062 (2014), 1401.2176.
[57] J. Erdmenger, N. Evans, and M. Scott (2014), 1412.3165.
[58] S. Matsuzaki and K. Yamawaki, Phys.Rev.Lett. **113**, 082002 (2014), 1311.3784.
[59] T. DeGrand and A. Hasenfratz, Phys.Rev. **D80**, 034506 (2009), 0906.1976.
[60] T. DeGrand, Phys.Rev. **D80**, 114507 (2009), 0910.3072.
[61] L. Del Debbio and R. Zwicky, Phys.Lett. **B700**, 217 (2011), 1009.2894.
[62] A. Patella, Phys.Rev. **D86**, 025006 (2012), 1204.4432.
[63] A. Cheng, A. Hasenfratz, G. Petropoulos, and D. Schaich, JHEP **1307**, 061 (2013), 1301.1355.
[64] A. Cheng, A. Hasenfratz, Y. Liu, G. Petropoulos, and D. Schaich, Phys.Rev. **D90**, 014509 (2014), 1401.0195.
[65] D. D. Dietrich, F. Sannino, and K. Tuominen, Phys.Rev. **D72**, 055001 (2005), hep-ph/0505059.
[66] G. 't Hooft, Nucl.Phys. **B138**, 1 (1978).
[67] J. Ambjorn, J. Giedt, and J. Greensite, JHEP **0002**, 033 (2000), hep-lat/9907021.
[68] G. Basar, A. Cherman, D. Dorigoni, and M. Unsal, Phys.Rev.Lett. **111**, 121601 (2013), 1306.2960.
[69] G. Basar, A. Cherman, and D. A. McGady (2014), 1409.1617.
[70] T. A. Ryttov and F. Sannino, Phys.Rev. **D78**, 115010 (2008), 0809.0713.
[71] S. Hands and S. E. Morrison (UKQCD Collaboration), Phys.Rev. **D59**, 116002 (1999), hep-lat/9807033.